Planophila laetevirens-Mediated Synthesis of Silver Nanoparticles: Optimization, Characterization, and Anticancer and Antibacterial Potentials

Reham Samir Hamida, Mohamed Abdelaal Ali, Njoud Mugren, Mayasar Ibrahim Al-Zaban, Mashael Mohammed Bin-Meferij, and Alya Redhwan*

ACCESS | 📊 Metrics & More | 📖 Article Recommendations

ABSTRACT: Algal-mediated synthesis of nanoparticles (NPs) opens the horizon for green and sustainable synthesis of NPs that can be used in many fields, such as medicine and industry. We extracellularly synthesized silver NPs (Ag-NPs) using the novel microalgae *Planophila laetevirens* under optimized conditions. The isolate was collected from freshwater/soil, purified, morphologically identified, and genetically identified using light, inverted light, scanning electron microscopy, and 18S rRNA sequencing. The phytochemicals in the algal extract were detected by GC−MS. Aqueous biomass extracts and cell-free media were used to reduce silver nitrate to Ag-NPs. To get small, uniformly shaped, and stable Ag-NPs, various abiotic parameters, including precursor concentration, the ratio between the reductant and precursor, temperature, time of temperature exposure, pH, illumination, and incubation time, were controlled during the synthesis of Ag-NPs. B-P@Ag-NPs and S-P@Ag-NPs (Ag-NPs synthesized using biomass and cell-free medium, respectively) were characterized using UV−vis spectroscopy, transmission electron microscopy, scanning electron microscopy, energy-dispersive X-ray analysis (EDX) and mapping, Fourier transform infrared (FTIR) spectroscopy, and a zeta sizer. S-P@Ag-NPs had a smaller size (10.8 ± 0.3 nm) than B-P@Ag-NPs (19.0 ± 0.6 nm), while their shapes were uniform quasispherical (S-P@Ag-NPs) and spherical to oval (B-P@Ag-NPs). EDX and mapping analyses demonstrated that Ag was the dominant element in the B-P@Ag-NP and S-P@Ag-NP samples, while FTIR revealed the presence of O−H, C−H, N−H, and C−O groups, indicating that polysaccharides and proteins acted as reductants, while polysaccharides/fatty acids acted as stabilizers during the synthesis of NPs. The hydrodynamic diameters of B-P@Ag-NPs and S-P@Ag-NPs were 37.7 and 28.3 nm, respectively, with negative charges on their surfaces, suggesting their colloidal stability. Anticancer activities against colon cancer (Sw620 and HT-29 cells), breast cancer (MDA-MB231 and MCF-7 cells), and normal human fibroblasts (HFs) were screened using the MTT assay. B-P@Ag-NPs and S-P@Ag-NPs had a greater antiproliferative effect against colon cancer than against breast cancer, with biocompatibility against HFs. The biocidal effects of the B-P@Ag-NPs and S-P@Ag-NPs were evaluated against *Escherichia coli*, *Bacillus cereus*, and *Bacillus subtilis* using agar well diffusion and resazurin dye assays. B-P@Ag-NPs and S-P@Ag-NPs caused higher growth inhibition of Gram-negative bacteria than of Gram-positive bacteria. B-P@Ag-NPs and S-P@Ag-NPs synthesized by *P. laetevirens* are promising antitumor and biocidal agents.
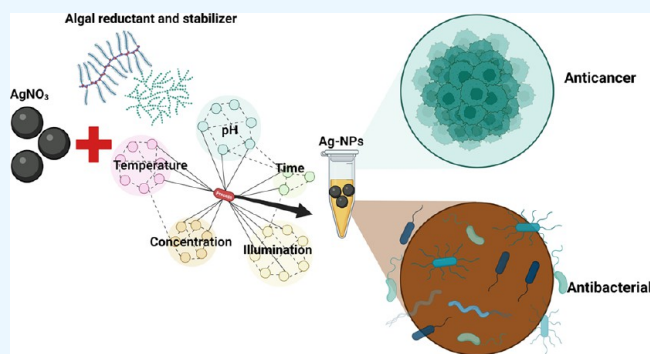
INTRODUCTION

Silver metal has received great attention since ancient times when Egyptian, Greek, Roman, and other civilizations used silver preparations to treat wounds and save food and water from spoilage.[1] Recently, scientists have produced a nanosize (1 dimension: 1−100 nm) of various metals with novel and unique physicochemical properties. Silver nanoparticles (Ag-NPs) have become one of the most attractive nanomaterials in the medical, pharmaceutical, and industrial fields owing to their unique characteristics including high reactivity, controlled size and shape, broad-spectrum activity, and highly efficient antimicrobial and anticancer activities.[2] The unique electro-

chemical and surface-enhanced Raman scattering features of Ag NPs enable their NPs to be utilized as biosensors for the detection of glucose, enzymes, proteins, and other molecules.[2] Because of their high reactivity, Ag-NPs have been used as

broad antimicrobial agents against Gram-positive and Gram-negative bacteria,[3] fungi,[4] and viruses,[5] as well as potent apoptotic enhancers in many cancers.[6] Ag-NPs can be produced using physical, chemical, or biological methods.[7] Although physical and chemical approaches are the most commonly used methods for synthesizing NPs, their limitations such as high production costs, low scalability, energy consumption, and high-yield toxic substances limit their use.[8] To address these issues, scientists have begun to use green synthesis to fabricate metals in the nanoform. One green method is biological synthesis, in which living cells are the source of reductants and stabilizing agents.[9] Many studies have demonstrated that microalgae,[10] cyanobacteria,[9] plants,[11] fungi,[12] lichens,[13] and others are greener biofactories for the bioreduction and stabilization of NPs.[11,14] Although bio-fabrication approaches result in less toxic NPs with no hazardous yield and low energy inputs, controlling the size and shape of NPs remains a major issue in biological synthesis methods. Researchers have recently reported computational and traditional optimization processes for NPs synthesis.[15] Changing the concentrations of precursors, temperature, pH, illumination conditions, and other abiotic and biotic factors mitigates the stability, shape, and size of NPs.[9,16] Additionally, researchers have found that synthesizing NPs using specific extracted biomolecules, such as pigments, enzymes, and proteins, regulates their shape and size.[17] Microalgae and cyanobacteria have many distinguishing characteristics that make them promising biofactories for NPs synthesis compared to other green synthesis routes. These characteristics include their higher growth rate, substantially higher rate of sequestering CO_2, hyperaccumulation of heavy metals, absence of toxic byproducts, minimum energy input, and employment of biomolecules (pigments and enzymes) as reducing and capping agents.[18] Many reports have demonstrated that microalgae have great potential for reducing and stabilizing NPs, such as Ag-,[19] Au-,[19] CuO-,[20] and TiO_2-NPs.[21] This is due to the ability of algae to remediate and detoxify heavy metals from their niches through phytochemical reactions and the use of chelating organic biomolecules.[22] The NPs produced by microalgae show great bioactivities, such as inhibitory potential against microbes and cancers,[23] antioxidant,[24] and wound repairing.[25] Ag-NPs synthesized by *Coelastrella aeroterrestrica* Strain BA_Chlo4 showed great anticancer activity against MCF-7, MDA, HCT-116, and HepG2 cells, with moderate toxicity against normal cells (HFs and Vero).[26] ZnO biosynthesized by *Chlorella vulgaris* showed significant antibacterial activity against resistant microbes, methicillin-resistant *Staphylococcus aureus*, and vancomycin-resistant *Enterococci*.[27] Gerneck isolated *Planophila laetevirens* for the first time from fresh water and soil in Europe in 1907.[30] *P. laetevirens* has a spherical to subspherical shape, and parietal chloroplasts cover roughly half of the cell interior with one obvious pyrenoid. Unfortunately, no reports have been published on the bioactivity, active metabolite analysis, or use of *P. laetevirens* for the synthesis of NPs. This study is the first to demonstrate the potential of *P. laetevirens* to reduce and stabilize Ag-NPs and to report the main phytochemicals of *P. laetevirens* that precipitate during the biofabrication of NPs. Additionally, this article describes two extracellular synthesis methods for Ag-NPs using *P. laetevirens* biomass extract and cell-free medium, as well as the optimum NPs synthesis conditions, including the influence of precursor concentrations and ratios, temperature, time of exposure to temperature, pH,

illumination, and incubation time, to produce stable, small, and uniform Ag-NPs. Finally, the physicochemical properties of the Ag-NPs and their anticancer and antibacterial activities were investigated. The use of *P. laetevirens* as biomachinery to synthesize Ag-NPs provides many advantages over other green synthesis methods, including using low concentration (2 mg/mL) of algal biomass to synthesize NPs, ability to synthesize AgNPs using their cell-free medium under dark condition, saving energy, and producing small, uniform controlled-size Ag-NPs with potent anticancer and antibacterial activities at lower concentrations and high biocompatibility comparing to other biogenic NPs.

■ MATERIALS AND METHODS

Isolation, Purification, and Cultivation of Microalgae. A sample was collected from soil immersed in rainwater, Riyadh, Saudi Arabia, kept in 50 mL falcons, and transferred to the laboratory to be kept in a sterile BG11-containing petri dish under a fluorescence lamp 2000 ± 200 lx (12:12 h dark/light cycle), at 20 °C for a week. The purification steps were performed as previously described by Bolch et al. and Hamida et al.[26,28]

Morphological Identification of Microalgae. During the algal culture, an aliquot (20 μL) of algal suspension was dropped on a thin glass slide and covered with a glass cover for light (Novex, Holland, The Netherlands) and inverted light microscopy (Thermo Fisher Scientific, USA) examination. The purified sample was centrifuged at 4700 rpm for 10 min and washed with distilled H_2O (dist. H_2O). Then, an aliquot of the algae was suspended in 70% ethanol, and 20 μL of the algal suspension was spread on a glass piece, dried at ambient temperature in a laminar flow, coated with platinum for 80 s using a platinum coater (JEC-3000FC, Joel, Tokyo, Japan), and examined with a scanning electron microscope (JSM-IT500HR, Joel, Japan) at 15 kV.[29]

18S rRNA Sequencing and Phylogenetic Tree. DNA was extracted from the purified algal pellets using a DNA extraction kit (Attogene, Austin, TX, USA) according to the manufacturer's instructions. PCR (PeqSTAR 96X universal gradient thermal cycler) was used to amplify the DNA according to Khaw et al.[30] with some modifications added as follows: initial denaturation step at 94.5 °C (with gradient ramping range of 0.5 deg) for 6 min, followed by 40 cycles of 95 °C for 30 s (denaturation step), 52 °C for 1 min (annealing step) and 74 °C for 1 min (extension), and final extension at 72 °C for 10 min. The forward primer CCTGGTTGATCCTGCCAG and reverse primer TTGATCCTTCTGCAGGTTCA were used for amplification. Amplicons were stored in nuclease-free water and sent to Macrogen (Seoul, Korea) for sequence analysis.

Preparation of Algal Extraction. In this study, two types of algal extracts: an aqueous biomass extract (i) and a cell-free medium (ii) of *P. laetevirens* were prepared. (i) After 15 days of algal culture, 1000 mL of the algal suspension was centrifuged at 4700 rpm for 10 min and the pellets were washed at least three times using distilled water (dist.H_2O. The cleaned pellets were kept at −80 °C overnight and freeze-dried using LYOTRAP (LTE Scientific, Greenfield, U.K.). The lyophiliza-tion period was dependent on the pellet size and algal nature; however, in general, the algae were converted to a dried powder over 48 h. The dried powder was vortexed for 1−2 min in the presence of glass beads (Sigma-Aldrich) to obtain a fine powder. Algal powder (500 mg) was dissolved in 250 mL of
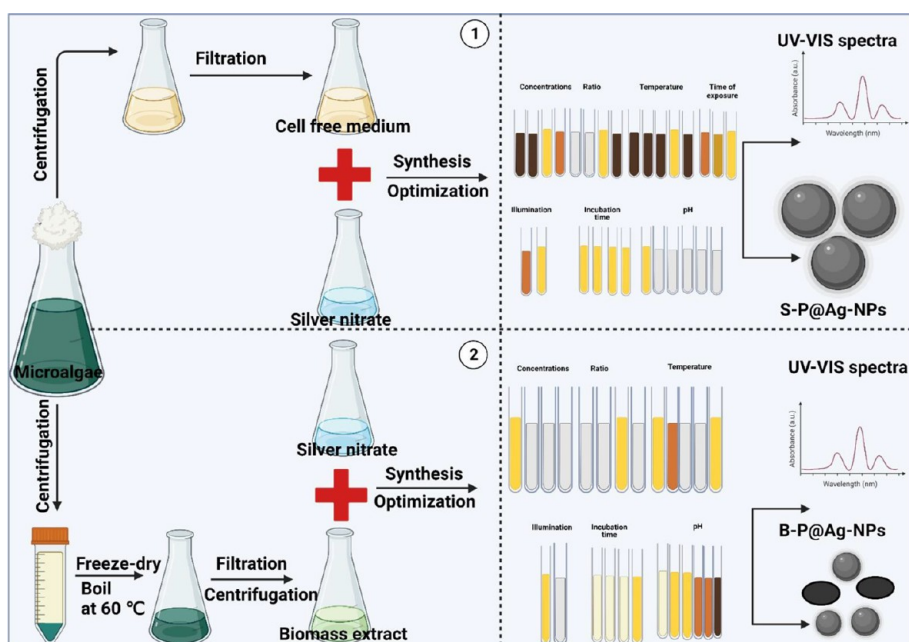
Figure 1. Synthesis of Ag-NPs using *P. laetevirens* cell-free medium (1) and biomass extract (2) by controlling the abiotic parameters including precursor concentrations and ratios, temperature, time of exposure to temperature, pH, illumination, and incubation time.

distilled water (2:1 algal powder to water) and was kept in a water bath at 60 °C for 30 min. The mixture was then cooled to room temperature, filtered by Whatman filter paper No.1, and the filtrate was centrifuged at 4700 rpm for 10 min to remove any debris. (ii) For the cell-free medium, a 30 day algal culture was centrifuged, and the supernatant was filtered using Whatman filter paper No. 1. Both extracts were used directly for NP synthesis and analysis.

Gas Chromatography−Mass Spectroscopy. A suspension of *P. laetevirens* (1 mg/mL) was boiled and sonicated for 30 min. Subsequently, the suspension was allowed to macerate for 24 h, centrifuged, followed by filtration with a syringe filter (0.22 μm), and the filtrate was dried under a vacuum at 50 °C for 48 h. To identify the volatile components in the prepared *P. laetevirens biomass* extract that may represent the stabilizer biomolecules in NP synthesis, a Trace GC-TSQ mass spectrometer (Thermo Scientific, Austin, TX, USA) with a direct capillary column TG−5MS (30 m × 0.25 mm × 0.25 μm film thickness) was used according to the method mentioned in our previous article.[26] The data were determined by comparing the mass spectra of the phytochemicals with those of the WILEY 09 and NIST 14 mass spectral databases.[31]

Optimization of Ag-NP Synthesis Using Microalgal Biomass and Supernatant. Two extracellular synthesis methods for Ag-NPs using *P. laetevirens* biomass extract and cell-free medium were performed by controlling the abiotic parameters, including precursor concentrations and ratios, temperature, time of exposure to temperature, pH, illumination, and incubation time to produce stable, small, and uniform Ag-NPs, as described in Figure 1.

Precursor Concentrations. To study the influence of precursor concentrations on the size and stability of NPs, 1 mL of cell-free medium or algal biomass extract was mixed with 4 mL of 1, 2, 4, and 5 mM AgNO₃ (Sigma Aldrich, USA) at 25 °C, under light, origin pH (without changing the pH of the reaction) for 24 h. After incubation, aliquots of the samples were analyzed using UV−vis spectroscopy. The optimum

concentrations were chosen based on the lowest wavelength values of the Ag-NPs in the range of 400−460 nm. Ag-NPs synthesized using a medium free of *P. laetevirens* are referred to as S-P@Ag-NPs, whereas those synthesized using the biomass extract are referred to as B-P@Ag-NPs. The optimum concentrations of AgNO₃ were 1 and 5 mM for B-P@Ag-NPs and S-P@Ag-NPs, respectively.

Ratio Change of Silver Nitrate Solution to Algal Extract. The effects of the algal extract and precursor ratio on the synthesis of S-P@Ag-NPs and B-P@Ag-NPs were investigated. B-P@Ag-NPs and S-P@Ag-NPs were synthesized by mixing algal extract or cell-free medium with optimum concentrations of AgNO₃ (1 and 5 mM) at different ratios of 1:1, 1:2, 1:4, 1:9 (V/V of algal extract to silver nitrate) at 25 °C, under light, and origin pH (without changing the pH of the reaction) for 24 h. The optimum algal extract-to-silver nitrate ratio for the synthesis of S-P@Ag-NPs and B-P@Ag-NPs was 1:4 V/V of algal extract to silver nitrate.

Influence of Temperature and Exposure Time on Silver NP Synthesis. A mixture of algal extract or cell-free medium was mixed with optimum concentrations of AgNO₃ at a 1:4 ratio and kept for 1 h at 40, 60, 80, and 100 °C. After 1 h of incubation, aliquots of the NP suspensions were analyzed using UV−vis spectroscopy. Notably, after 1 h of incubation, the S-P@Ag-NP suspension converted to orange-brown color, whereas the B-P@Ag-NPs showed no response to temperature change and were colorless. Thus, B-P@Ag-NPs were kept under light for 24 h at 25 °C. The optimum temperature of S-P@Ag-NPs and B-P@Ag-NPs were 80 and 25 °C, respectively. For S-P@Ag-NPs, 1 mL of cell-free medium was mixed with 4 mL of 5 mM AgNO₃ at 80 °C for 15, 30, and 60 min to assess the influence of time exposure to heat energy on NP synthesis.

Influence of Illumination and Incubation Time on Ag-NP Synthesis. Under optimal conditions, an algal extract or cell-free medium mixture was mixed with AgNO₃ and kept under light and once under dark. The optimum illumination conditions for S-P@Ag-NPs were dark incubation, whereas

those for B-P@Ag-NPs were maintained under light conditions. We studied the influence of incubation time on the size and stability of the NPs by maintaining a mixture of algal extract or cell-free medium and $AgNO_3$ in the dark (for S-P@Ag-NPs) or light (for B-P@Ag-NPs) for 1, 3, 12, and 24 h.

Influence of pH on Ag-NP Synthesis. The variation in pH during the synthesis of both B-P@Ag-NPs and S-P@Ag-NPs was studied by adding an algal extract or cell-free medium to $AgNO_3$ and adjusting the reaction pH to be 6, 7, 8, 9, and 12 using HCL or NaOH (0.1 M) (Sigma Aldrich, USA). Additionally, the pH of algal extract or cell-free medium to $AgNO_3$ reactions was measured and kept unchanged (pH origin). The optimum conditions for S-P@Ag-NPs and B-P@Ag-NPs synthesis were at 1 mL of algal extract or cell-free medium to 4 mL of $AgNO_3$ (1 and 5 mM for B-P@Ag-NPs and S-P@Ag-NPs, respectively) at 80 °C, dark incubation for 1 h (for S-P@Ag-NPs) and at 25 °C, light incubation for 24 h (for B-P@Ag-NPs) at pH origin.

Physicochemical Characterization of Optimum Ag-NPs. *UV−Vis Spectroscopy.* Generally, a 2 mL aliquot of the Ag-NP suspension at each optimization condition was scanned using UV−vis spectroscopy (Shimazu, Japan) using a wavelength range of 200−800 nm and a resolution of 1 nm.

Fourier Transform Infrared and Zeta Sizer. The functional groups on the NPs surfaces and their extracts were determined in the range of 400−4000 cm^{-1} using Fourier transform infrared (FTIR) spectroscopy (Shimadzu, Kyoto, Japan). The hydrodynamic diameters and potential charges of the S-P@Ag-NPs and B-P@Ag-NPs were measured using a Zetasizer instrument (Malvern, U.K.). In brief, 500 μg were dissolved in 1 mL of distilled water at pH 7, sonicated for 30 min, 10-fold diluted, sonicated for 2 min, and transferred to Zeta sizer tubes for measurements.

Transmission and Scanning Electron Microscopy, Energy-Dispersive X-ray Analysis, and Mapping Analyses. Transmission electron microscopy (TEM; EM-1400Flash, Joel, Tokyo, Japan, 120 kV), SEM (scanning electron microscopy), energy-dispersive X-ray analysis (EDX), and mapping analysis (JSMIT500HR, STD-PC80, Joel, Tokyo, Japan) were used to investigate the shape, size, elemental composition, and distribution of the S-P@Ag-NPs and B-P@Ag-NPs. The samples were prepared according to the method described in our previous article.[16]

Anticancer Activity of Ag-NPs. Colon cancer cell lines (Sw620 and HT-29), breast cancer cell lines (MDA-MB231 and MCF-7), and the normal human fibroblast cell line (HFs) were obtained from American Type Culture Collection (ATCC, Manassas, VA, USA) and cultured in RPMI (HT-29) and DMEM supplemented by 10% FBS, and 50 U/mL penicillin and streptomycin and kept at 37 °C in a 5% CO_2 incubator until 75% confluency. Drug preparation:1 mg of S-P@Ag-NPs, B-P@Ag-NPs, Ch@Ag-NPs, and 5-fluorouracil (5-FU; Sigma Aldrich, USA) were mixed with 1 mL cell culture media, and the NP suspensions were sonicated for 15 min in an ultrasonic bath (Grant, UK). The 5-FU solution was vortexed for 1 min. All suspensions were filtered through a 0.45 μm syringe filter for direct application to cells. The MTT assay was used to estimate the anticancer activities of S-P@Ag-NPs, B-P@Ag-NPs, Ch@Ag-NPs, and 5-FU (as a positive control) against Sw620, HT-29, MCF-7, MDA-MB-231, and HFs. Notably, 5-FU and Ch@Ag-NPs were assessed only against Sw620 and HT-29 cells, while MCF-7, MDA-MB-231, and HFs were assessed and published in our previous articles.[16,26]

The cells (5×10^4 cells/mL) were cultured in 96-well plates and kept in a 5% CO_2 incubator for 24 h at 37 °C until they reached 75% confluency and the cells were treated with serial dilutions of S-P@Ag-NPs and B-P@Ag-NPs at 200.0, 100.0, 50.0, 25.0, 12.5, 6.25, 3.13, 1.56, and 0.78 μg/mL, and 1000, 500, 250, 125, 62.5, 31.25, 15.62, 7.81, and 3.90 μg/mL of Ch@Ag-NPs and 5-FU. Then, the plates were incubated for 24 h in a 5% CO_2 incubator at 37 °C. The MTT assay was performed according to the method described by Mosmann and the plates were read using a plate reader at 570 nm. Cell viability (%) was estimated using the following equation:[16,32]

$$(Abs(treated)/(Abs(control)) \times 100$$

The IC_{50} (half-maximal growth inhibitory concentration) was calculated from a sigmoidal curve.

Antimicrobial Activity of Ag-NPs. Gram-negative bacteria *Escherichia coli* and Gram-positive bacteria *Bacillus cereus* and *Bacillus subtilis* were obtained from the Department of Microbiology, King Saud University, Riyadh, Saudi Arabia, and cultured in a nutrient broth for up to 18 h at 37 °C and maintained by continuously subculturing them in broth and on agar media. The agar-well diffusion approach was used to assess the antimicrobial activity of 1 mg/mL of S-P@Ag-NPs, B-P@Ag-NPs, chemically synthesized Ag-NPs (Ch@Ag-NPs), and 5 μg/mL ciprofloxacin against all tested bacteria as follows: 4 mL of the bacterial suspension ($2.5-3.6 \times 10^6$ CFU/mL) was suspended in 50 mL of nutrient agar media. The mixture was poured into sterile Petri dishes and dried at 37 °C. 8 mm wells were created on the agar plates using a cork borer. Subsequently, 100 μL of S-P@Ag-NPs, B-P@Ag-NPs, Ch@Ag-NPs, and ciprofloxacin suspensions were poured into the 8 mm wells. The plates were placed in a bacterial incubator at 37 °C for 24 h. The diameter of the inhibition zone (mm) was estimated using a transparent ruler.[33]

Minimum Inhibition and Bactericidal Concentrations. Minimum inhibitory and bactericidal concentrations (MIC and MBC) of algal extract, S-P@Ag-NPs, and B-P@Ag-NPs were determined using the resazurin dye method described by Elshikh et al.[34] In summary, 100 μL of nutrient broth medium was added to each well of a 96-well plate, beginning with column 2 and continuing to column 12. Next, 100 μL of algal extract, S-P@Ag-NPs, and B-P@Ag-NPs at a concentration of 1 mg/mL were dispensed into the wells in triplicate in column 1, and various concentrations were prepared across the plate to column 10 using the serial dilution method. These concentrations included 500, 250, 125, 62.5, 31.25, 15.62, 7.8, 3.9, 1.95, and 0.98 μg/mL. Next, 100 μL of bacterial suspension with a concentration of ($2.5-3.6 \times 10^6$ CFU/mL) was placed into each well. Column 11 served as the positive control, which consisted of an untreated bacterial suspension, whereas column 12 served as the negative control (medium only to monitor sterility). After that, the plates were kept in the incubator overnight at 37 °C. The resazurin dye solution was prepared by dissolving 0.015 g of resazurin in 100 mL of distilled water, vortexing the mixture for 10 min, and filtering it through a microfilter with a pore size of 0.45 μm. After 24 h, 30 μL/well of resazurin dye solution was added, and the plate was kept at 37 ° C for a period of 4 h. Absorbance was measured at 570 nm using a plate reader (Hercules, CA, USA). After 4 h, the column was considered above the MIC value if there was no color change (the color of the resazurin indicator, blue, remained the same). The MBC values were calculated by depositing the contents of wells with concentrations greater

than the MIC on nutrient agar plates. The MBC values indicated the lowest concentration of the drug at which the plates did not show any signs of colony growth.

Statistical Analysis. GraphPrism version 9.3.1 (GraphPad Software Inc., San Diego, CA, USA), Origin 8 (OriginLab Corporation, Northampton, MA, USA), and ImageJ (National Institutes of Health, Bethesda, MD, USA) software were used to analyze and demonstrate the data. All data were produced from separated experiments in triplicate and expressed as a mean ± SEM.

RESULTS AND DISCUSSION

Microscopic Examination of *P. laetevirens*. Light and inverted light microscopes, as well as a scanning electron microscope, were used to examine the morphology of *P. laetevirens* (Figure 22−F). *P. laetevirens* was found to be either
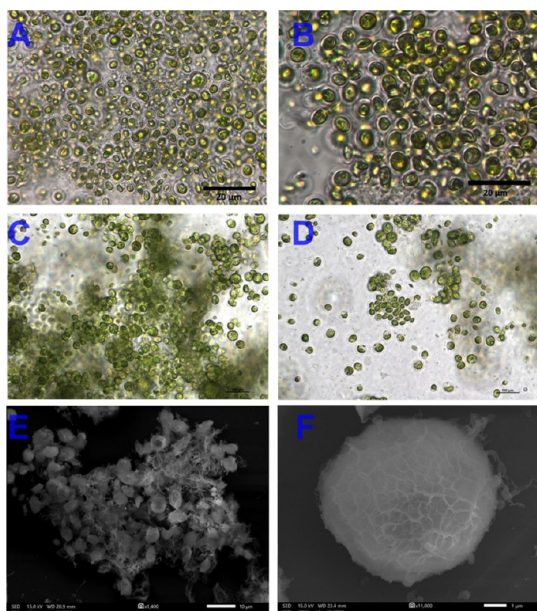
Figure 2. Light (A, B), inverted light (C, D), and scanning electron microscopy (E, F) micrographs of *Planophila laetevirens* SAG 2008 demonstrating the brownish-green color, spherical-to-subspherical shape, and parietal chloroplasts each with one obvious pyrenoid. Scale bar of 20 μm (A, B), 100 μm (C, D), 10 μm (E), and 1 μm (F).

solitary or in groups (2−8 cells) with no surrounding protruding gelatinous envelopes. *P. laetevirens* has a brownish-green color, spherical-to-subspherical shape, and parietal chloroplasts with one clear pyrenoid and many large vegetative cells, which were also detected. SEM micrographs showed that *P. laetevirens* had irregular surfaces and was trapped in web-like biomaterials. *P. laetevirens* in aqueous BG11 appeared as a piece of green paper that was not easily loosened by shaking, as shown in Figure 1C. Gerneck isolated and identified *P. laetevirens* for the first time in 1907.[35] The scientist reported that *P. laetevirens* was spherical or subspherical with a cell size of <10.5 μm and had parietal chloroplast covering roughly half of the cell interior with one obvious pyrenoid. *P. laetevirens* have 1−2 cytoplasmic vacuoles. Vegetative (mother) cells split into two daughter cells that split quickly after division. The resulting zoospores were more than 6 m (length) and 7.5 m (width), with a posterior cup-shaped chloroplast and lateral eyespot.

18S rRNA. Sequence analysis showed that the isolated species had 99.8% similarity to *P. laetevirens* SAG 2008 with a query recovery of 98%. The species was recorded in GenBank, NCBI, with the accession number OQ564446. The phylogenetic tree showed that the isolate might cluster within *Planophila* (Figure 3).
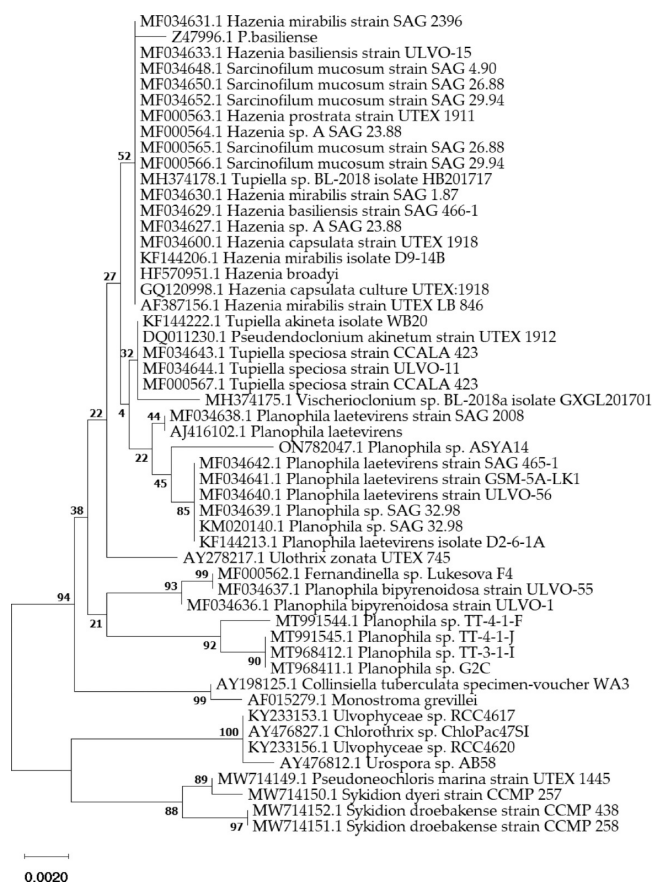

Figure 3. Phylogenetic tree of *Planophila laetevirens* SAG 2008 inferred from 18S rRNA and constructed by cluster method using MEGA4 software version 10.2.6. The number at each branch refers to the bootstrap values for % of 1000 replicate trees calculated by the neighbor-joining method.

Chemical Composition of Aqueous Extract of *P. laetevirens*. The chemical composition determined by GC−MS demonstrated that the volatile components present in the aqueous extract of *P. laetevirens* were fatty acids and esters (Figure 4 and Table 1). It was found that *P. laetevirens* was rich in important fatty acids, such as linoelaidic acid, stearic acid, and 2-monoolein, which have several medical and industrial applications. For instance, 2-monoolein has been used as a drug vehicle for managing chronic lung diseases, whereas stearic acid regulates mitochondrial morphology and function.[36] Algal fatty acids and esters may have acted as stabilizing agents, preventing NP oxidation and agglomeration during the synthesis of S-P@Ag-NPs and B-P@Ag-NPs.[37]

Optimization Process of Ag-NPs Synthesis Using *P. laetevirens* Biomass and Cell-Free Medium. *Influence of Various Concentrations and Ratios of Silver Nitrate on Ag-NP Synthesis.* The influence of AgNO3 concentration on the synthesis process of both S-P@Ag-NPs and B-P@Ag-NPs at constant ratios 1:4 (V/V of algal extract to precursor solution), 25 °C, light, for 24 h and without changing the pH was
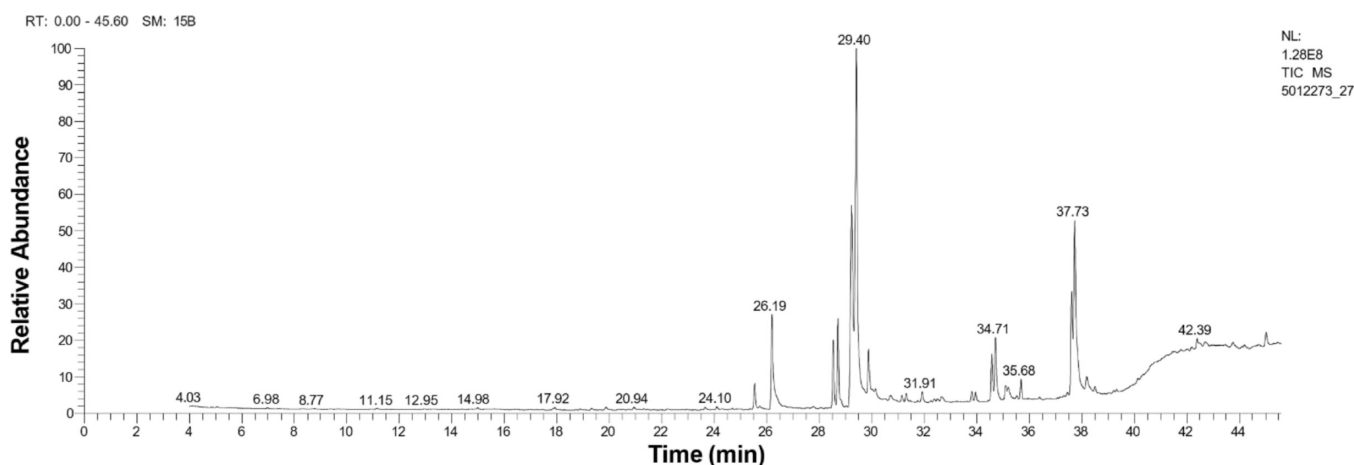
Figure 4. GC−MS chromatograph of phytochemicals detecting in *P. laetevirens* biomass extract.

assessed using UV−vis spectroscopy (Figure 5). Intriguingly, increasing the AgNO$_3$ concentration blue-shifted the wavelength of S-P@Ag-NPs. The data showed that 5 mM AgNO$_3$ resulted in the formation of S-P@Ag-NPs with shorter wavelengths at 444 nm compared to 1, 2, and 4 mM at 464 and 446 nm, respectively. In contrast, 4 mL of 1 mM AgNO$_3$ was the optimum concentration for reduction by 1 mL of algal extract to B-P@Ag-NPs at 411 nm, whereas other concentrations of 2, 4, and 5 mM were not reduced by the algal extract to B-P@Ag-NPs. When the concentration of AgNO$_3$ was increased, the reductant concentration was insufficient to reduce silver nitrate to B-P@Ag-NPs. Therefore, we can conclude that the increase or decrease in the AgNO$_3$ concentration depends on the reductant concentration to achieve a balanced reduction reaction. Sobczak-Kupiec et al. found that increasing the concentration of silver nitrate increased the NP size and aggregation.[38] After determining the optimum concentrations of AgNO$_3$ for the reduction of both S-P@Ag-NPs and B-P@Ag-NPs, the effect of ratio variation on the synthesis process was investigated (Figure 5). S-P@Ag-NPs were synthesized by mixing the algal extract with 5 mM AgNO$_3$ at 1−1, 1−2, 1−4, and 1−9 (V/V). The B-P@Ag-NPs were synthesized by mixing the algal extract with 1 mM AgNO$_3$ at 1−1, 1−2, 1−4, and 1−9. The data revealed that the optimum ratio for the synthesis of S-P@Ag-NPs and B-P@Ag-NPs was 1−4 at wavelengths of 444 and 411 nm, respectively. Other ratios either resulted in agglomerated NPs or were unsuitable for the NPs synthesis process.[39]

Influence of Temperature and Time of Exposure to Temperature on Ag-NP Synthesis. The influence of temperature on the synthesis process of S-P@Ag-NPs and B-P@Ag-NPs was conducted by mixing 1 mL of the algal extract with 4 mL of either 5 or 1 mM AgNO$_3$ at 25, 40, 60, 80, and 100 °C. The data showed that the optimum temperatures for the biofabrication of S-P@Ag-NPs and B-P@Ag-NPs were at 80 and 25 °C at wavelengths of 423 and 411 nm, respectively (Figure 5). Intriguingly, increasing the temperature to 40 and 60 °C caused a red shift in the wavelength of S-P@Ag-NPs to 447 nm, while an increase to 80 °C resulted in a blue shift from 444 (25 °C) to 423 nm (80 °C). However, increasing the temperature to 100 °C produced nonuniform NPs at wavelengths of 424, 411, and 402 nm. On the other hand, increasing the temperature from 25 to 40 °C caused an increase in the wavelength of B-P@Ag-NPs from 411 to 430 nm, while at 60 and 80 °C, NPs did not form. The temperature

at 100 °C did not affect the wavelengths of B-P@Ag-NPs, which were 412 nm, which was similar to that of B-P@Ag-NPs synthesized at 25 °C. To test the influence of time of exposure to temperature on the particle size and stability, 1 mL of algal extract was mixed with 4 mL of either 5 mM AgNO$_3$ at 80 °C for 15, 30, and 60 min. The data demonstrated that by increasing the time of incubation at 80 °C, smaller NPs formed (Figure 5). For instance, the wavelengths of the S-P@Ag-NPs were 443, 438, and 423 nm at 15, 30, and 60 min, respectively. A possible explanation is that an increase in temperature to a certain degree activates the reductants (biomolecules) during the synthesis of NPs, while raising the temperature beyond the optimum degree could result in biomolecule degradation and the formation of agglomerated NPs or stop the reduction reaction. It was found that the formation of NPs at higher temperatures might be due to an increase in the nucleation kinetics constant instead of a decreased growth kinetics constant, considering the concentrations of the precursors.[40] An increase in the reaction temperature caused the rapid formation of Ag clusters and reduced the concentration of the Ag precursor. Hence, uniform Ag-NPs were formed with a rapid reduction rate.[41]

Influence of Illumination and on Time of Exposure Ag-NP Synthesis. The data showed that the optimum condition to synthesize S-P@Ag-NPs was keeping the reaction in the dark after exposing to 1 h of 80 °C (423 nm) while exposing the reaction to light caused an increase in nanosize and agglomeration of NPs (440 nm). In contrast, in the dark, the algal biomass extract did not reduce silver nitrate to B-P@Ag-NPs (Figure 5), whereas light incubation was the optimum condition for the synthesis of B-P@Ag-NPs (411 nm). These data suggest that the bioreduction of silver nitrate by algal extracts is a photoreduction process, in which light plays a significant role in activating the reduction process.[42] To determine the influence of incubation time on the NPs suspension, mixtures of algal extract and silver nitrate were kept at optimum conditions of concentration, ratio, temperature, pH, and illumination for 1, 3, 12, and 24 h. The data demonstrated that the SPRs of S-P@Ag-NPs changed slightly with time. For instance, the wavelengths of the S-P@Ag-NPs at 1, 3, 12, and 24 h were 423, 423.5, 425, and 425.5 nm suggesting their stability. On the other hand, the wavelength of B-P@Ag-NPs decreased from 418 to 411 nm as the incubation time increased from 1, 3, 12, and 24 h, suggesting that more time of light exposure increased the reduction rate of NPs,

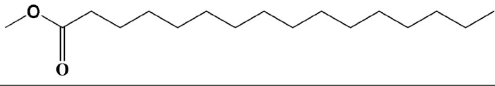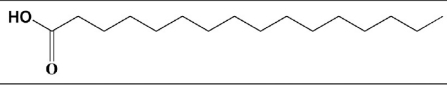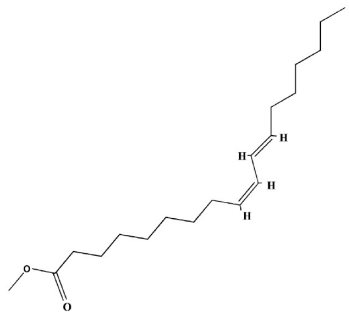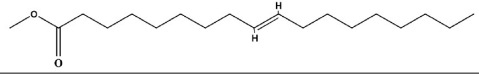**Table 1. Phytochemicals Detecting in *P. laetevirens* Biomass Extract Using GC−MS**
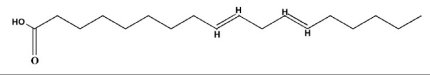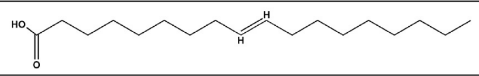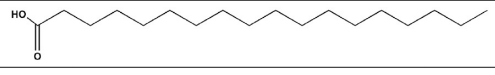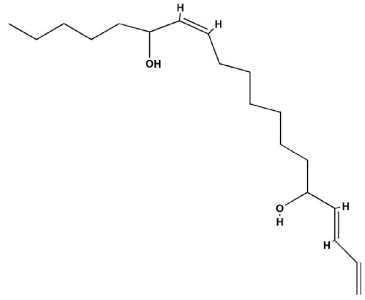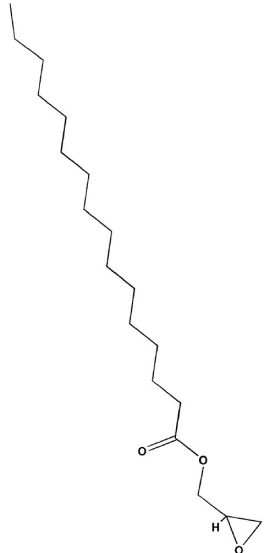
No.	Compound	Retention Time	Area%	Matched Factor	Molecular Formula	Molecular Weight	Chemical Structure
1	Methyl palmitate	25.53	1.75	915	$C_{17}H_{34}O_2$	270	
2	n-Hexadecanoic acid	26.19	6.65	914	$C_{16}H_{32}O_2$	256	
3	Bovinic acid methyl ester	28.53	4.56	928	$C_{19}H_{34}O_2$	294	
4	Methyl elaidate	28.71	6.39	918	$C_{19}H_{36}O_2$	296	
5	Linoelaidic acid	29.22	16.01	934	$C_{18}H_{32}O_2$	280	
6	Elaidic acid	29.41	24.07	936	$C_{18}H_{34}O_2$	282	
7	Stearic acid	29.87	3.19	904	$C_{18}H_{36}O_2$	284	
8	E,E,Z-1,3,12-Nonadecatriene-5,14-diol	31.31	0.59	776	$C_{19}H_{34}O_2$	294	
9	Glycidyl palmitate	31.91	0.80	856	$C_{19}H_{36}O_3$	312	

Table 1. continued
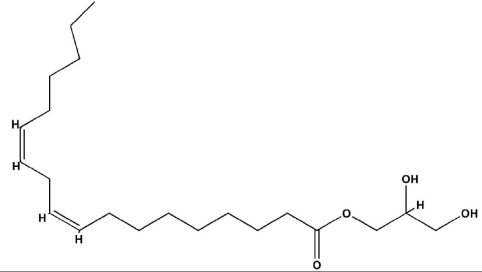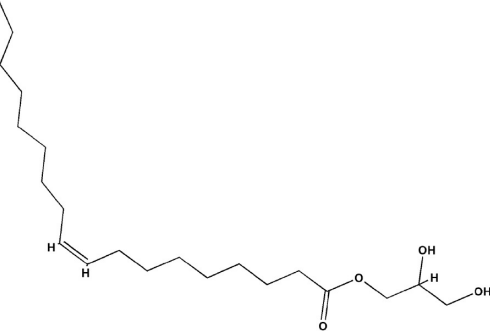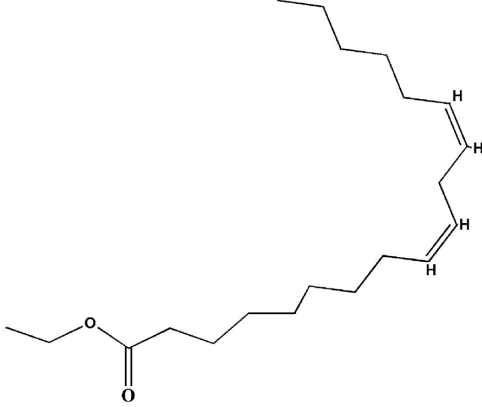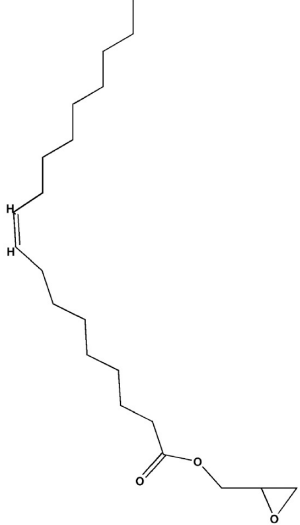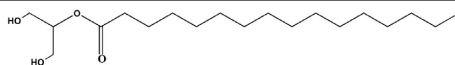
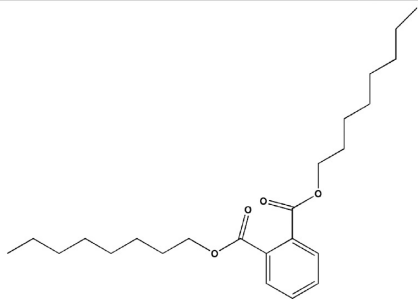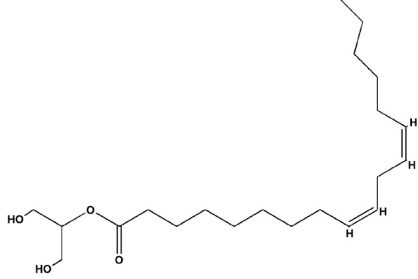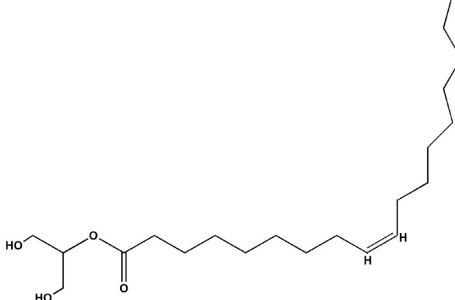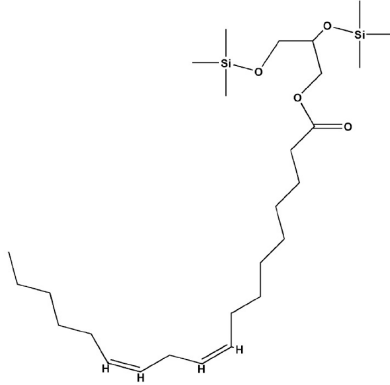| No.	Compound	Retention Time	Area%	Matched Factor	Molecular Formula	Molecular Weight	Chemical Structure
10	Glyceryl monolinoleate	33.80	0.72	793	$C_{21}H_{38}O_4$	354	
11	Glyceryl monooleate	33.95	0.64	834	$C_{21}H_{40}O_4$	356	
12	Ethyl linoleate	34.56	3.35	856	$C_{20}H_{36}O_2$	308	
13	Glycidyl oleate	34.70, 35.19, 38.17	4.67, 1.06, 1.10	912 ,791, 783	$C_{21}H_{38}O_3$	338	
14	2-Palmitoylglycerol	35.09	1.04	859	$C_{19}H_{38}O_4$	330	

Table 1. continued

No.	Compound	Retention Time	Area%	Matched Factor	Molecular Formula	Molecular Weight	Chemical Structure
15	Phthalic acid, dioctyl ester	35.68	1.35	820	$C_{24}H_{38}O_4$	390	
16	2-Linoleoylglycerol	37.60	7.10	888	$C_{21}H_{38}O_4$	354	
17	2-Monoolein	37.72	13.04	879	$C_{21}H_{40}O_4$	356	
18	Linoleic acid, 2,3-bis-(O-TMS)-propyl ester	42.39, 45.02	0.66, 1.23	785, 780	$C_{27}H_{54}O_4Si_2$	498	

resulting in smaller NPs. To sum up, the S-P@Ag-NPs were optimum synthesized at 5 mM of silver nitrate, 1:4 (V/V algal extract to silver nitrate), 80 °C for 1 h, dark incubation, pH 7.4, while B-P@Ag-NPs were optimum synthesized at 1 mM, 1:4 (V/V algal extract to silver nitrate), 25 °C, light incubation, pH 7 for 24 h. The SPRs of S-P@Ag-NPs and B-P@Ag-NPs under the optimum conditions were 423 and 408.5 nm. These peaks correspond to the localized surface plasmon resonance of the Ag-NPs.[43]

Influence of pH on Ag-NP Synthesis. S-P@Ag-NPs were optimally synthesized without changing the pH, and the original reaction pH was 7.4. The SPR peak of S-P@Ag-NPs was observed at 423 nm. When the pH of the S-P@Ag-NPs

reaction was changed to 6, 7, 8, 9, or 12, NPs were not synthesized. In contrast, B-P@Ag-NPs showed enhanced SPR (408.5 nm) and intensity at an optimum pH of 7 compared to pH 6 (396 nm), the origin pH 6.3 of the reaction (411 nm), pH 8 (414.5 nm), pH 9 (457 nm), and pH 12 (412 and 439 nm). These data demonstrate that a natural pH of approximately pH 7 is the optimum pH for the synthesis of both S-P@Ag-NPs and B-P@Ag-NPs with small nanosize and good stability (Figure 5). It was found that Ag-NPs were less aggregated at pH levels between <3 and >7 because all groups were protonated at pH levels below 3, working against electrostatic interactions. At pH greater than 7, all groups were deprotonated, favoring repulsion between the NPs and
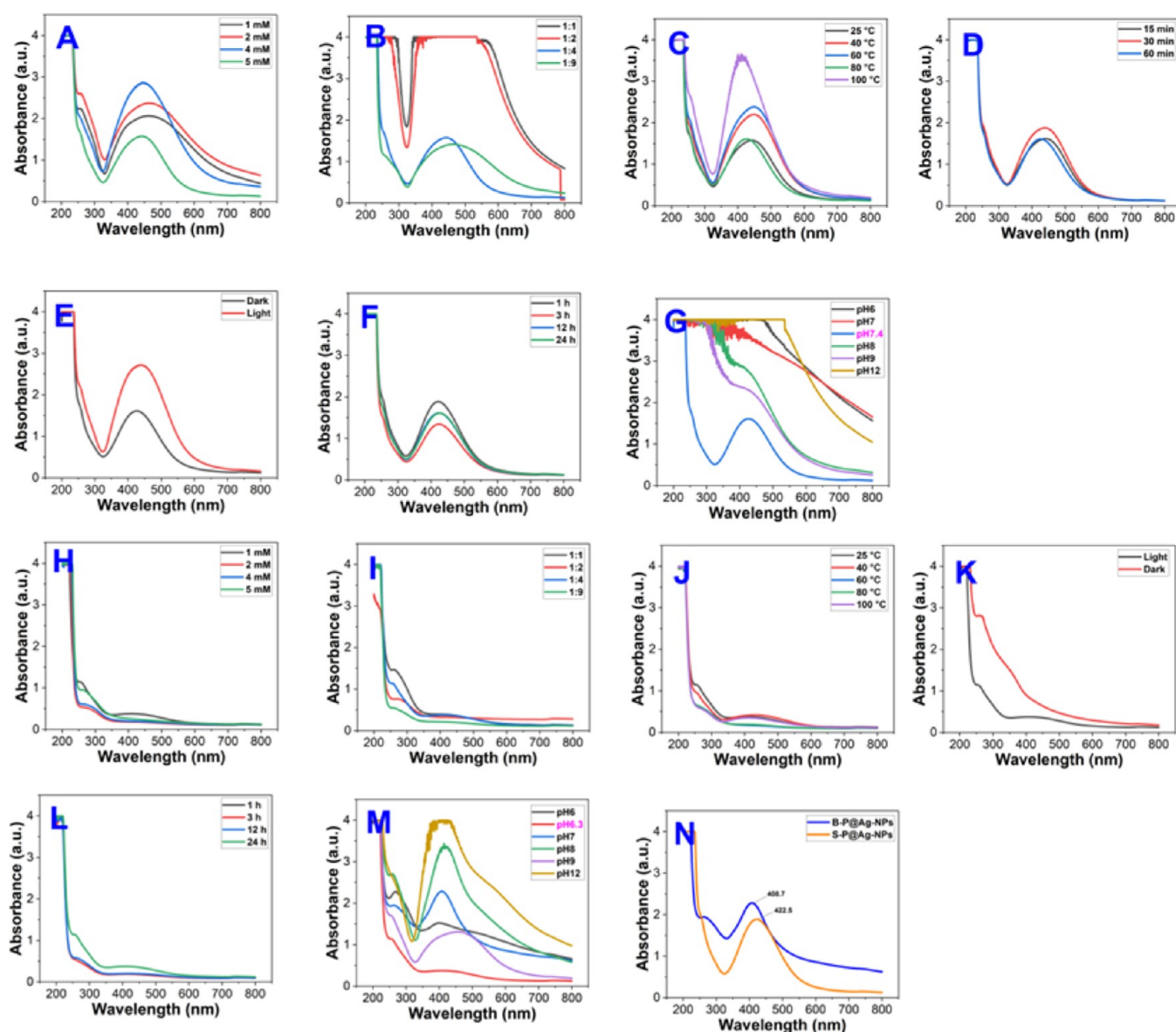
Figure 5. UV−VIS spectra of S-P@Ag-NPs (A−G) and B-P@Ag-NPs (H−M) synthesized by cell-free medium and *P. laetevirens* biomass extract at various concentrations (A, H), ratio (B, I), temperature (C, J), time of exposure to temperature (D), illumination conditions (E, K), time of incubation (F, L), pH (G, M), and the final SPR of S-P@Ag-NPs and B-P@Ag-NPs at optimum conditions (N).

discouraging aggregation.[44] According to Zhao et al., at higher pH values, the electrostatic interactions between the negatively charged functional groups such as carboxyl groups, and the positively charged silver ions become stronger.[45] To summarize, the optimum conditions for synthesizing S-P@Ag-NPs and B-P@Ag-NPs were 5 mM AgNO₃, 1:4, 80 °C for 1 h, incubation in dark for 1 h at pH 7.4; and 1 mM AgNO₃, 1:4, 25 °C, incubation under light for 24 h at pH 6.3; respectively.

TEM and SEM. The TEM micrographs of S-P@Ag-NPs and B-P@Ag-NPs demonstrated that the S-P@Ag-NPs mostly had a spherical-to-quasi-spherical shape with a small size and no agglomeration (Figure 6). The B-P@Ag-NPs had an oval-to-spherical shape with a small nanosize. However, the B-P@Ag-NPs appeared to be steaky in the organic algal matrix, which could be polysaccharides, lipids, or proteins. However, increasing the magnification of the B-P@Ag-NPs revealed that most of the particles were separated from each other, but

were trapped in a matrix-like web. The frequency distribution revealed that the particle size of S-P@Ag-NPs (10.8 ± 0.3 nm) was smaller than that of B-P@Ag-NPs (19.0 ± 0.6 nm). SEM micrographs of *P. laetevirens* showed that the algal cells were surrounded by a condensed biomaterial matrix. Similarly, the SEM micrographs revealed that the S-P@Ag-NPs and B-P@Ag-NPs had spherical shapes and small sizes (Figure 7). Gallón et al. synthesized Ag-NPs using polysaccharides from *Botryococcus braunii* and *Chlorella pyrenoidosa* and found that the size was between 5 and 15 nm and had a spherical shape.[46]

EDX and Mapping Analyses. EDX and mapping analyses were performed to determine the chemical composition of S-P@Ag-NPs and B-P@Ag-NPs (Figures 8 and 9, and Table 2). The data demonstrated that silver was the most dominant element in both NP samples with 55.6% for S-P@Ag-NPs and 75% for B-P@Ag-NPs,[46] whereas oxygen (23.47%) and chloride (9.9%) were the second most dominant elements in S-P@Ag-NPs and B-P@Ag-NPs, respectively. Other trace
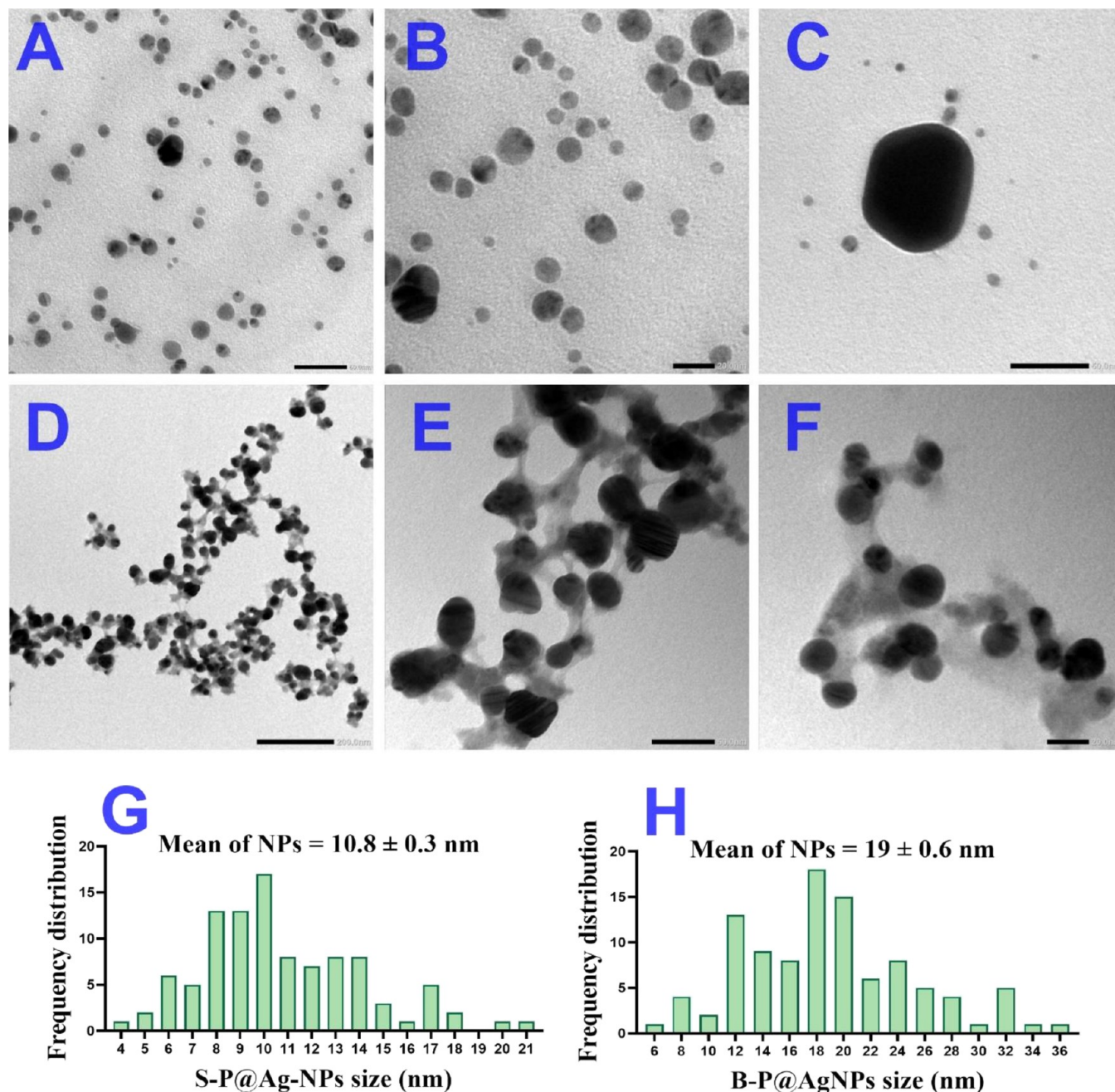
Figure 6. TEM micrographs of S-P@Ag-NPs (A−C) and B-P@Ag-NPs (D−F) synthesized by cell-free medium and *P. laetevirens* biomass extract and frequency distribution histogram of S-P@Ag-NPs (G) and B-P@Ag-NPs (H). Scale bar of 50 (A, C, E), 20 (B, F), and 200 nm (D).

elements were detected, including phosphorus, zinc, copper, zirconium, sulfur, sodium, aluminum, and silica. The existence of elements such as copper could be the result of using a copper stub for sample preparation, while other trace elements such as Si ($C_{27}H_{54}O_4Si_2$ detected by GC−MS analysis), P, Zr, S, and Na could emerge from the algal materials, as these elements are important for algal growth and metabolism.[47] Unexpectedly, C atoms were not detected by EDX in S-P@Ag-NPs but appeared after mapping analysis.

Zeta Sizer. The hydrodynamic diameters of B-P@Ag-NPs and S-P@Ag-NPs in the aqueous system were 37.7 and 28.3 nm, respectively, with PDIs of 0.55 and 0.56 (Figure 10 and Table 3). The HDs of both B-P@Ag-NPs and S-P@Ag-NPs were similar to the particle sizes of B-P@Ag-NPs and S-P@Ag-

NPs measured using ImageJ software based on TEM micrographs. Interestingly, the HD of S-P@Ag-NPs was smaller than that of B-P@Ag-NPs, which could be due to the presence of more algal corona surrounding B-P@Ag-NPs, which could adsorb more water molecules or stack the particles together (Figure 4), causing an increase in HD values. Additionally, the potential charges on B-P@Ag-NPs and S-P@Ag-NPs surfaces were −28.4 and −26.1 mV, respectively (Figure 10). These data suggest that B-P@Ag-NPs and S-P@Ag-NPs are stable in colloidal systems. Additionally, the negativity of the NP surfaces could be derived from biomolecules surrounding the NPs, such as COO- and OH.[48] Roychoudhury et al. synthesized Ag-NPs using *Lyngbya*
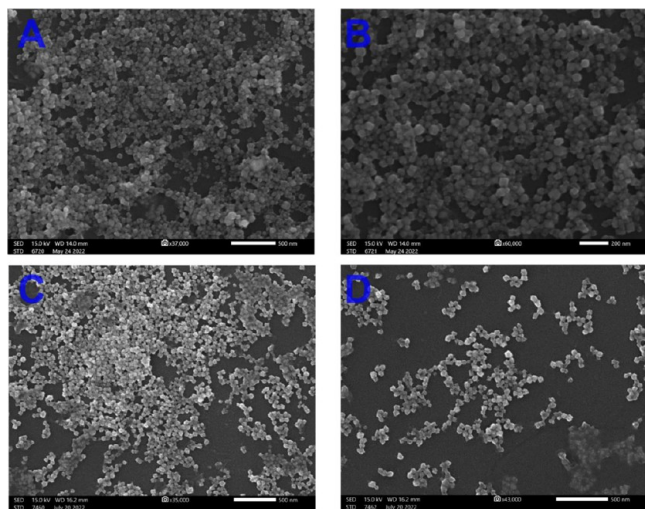
Figure 7. SEM micrographs of S-P@Ag-NPs (A, B) and B-P@Ag-NPs (C, D) synthesized by cell-free medium and *P. laetevirens* biomass extract. Scale bar of 200 (B) and 500 nm (A, C, D).

majuscule and found that their HD and zeta potentials were 149 nm and −35.2 mV.[49]

FTIR. The FTIR spectra of *P. laetevirens* biomass extract, cell-free medium, S-P@Ag-NPs, and B-P@Ag-NPs are shown in Table 4 and Figure 11. These data demonstrate that the main functional groups in *P. laetevirens* biomass extract and cell-free medium were O−H, followed by C−H, C−O, C=O, N−H, N−O, C=C, C−N, and S=O bonds, indicating that organic molecules such as polysaccharides, fatty acids, and proteins may be involved in the synthesis of NPs. However, *P. laetevirens* biomass extract contained more functional groups than the cell-free medium. For instance, the O−H spectra of *P.*

laetevirens biomass were detected in many spectra at 3834.4, 3746.3, 3563.4, and 3280.0 cm^{-1}, while the cell-free medium had only one spectrum at 3740.6 cm^{-1} corresponding to O−H. Moreover, it was found that *P. laetevirens* biomass extract had N−O, COO$^-$ and C=C−C groups which were not detected in the cell-free medium, while the cell-free medium had other groups S−C≡N and C−N groups. By examining the functional groups surrounding both S-P@Ag-NPs and B-P@Ag-NPs, it was found that the main groups on their surfaces included O−H, C−H, N−H, and C−O, suggesting that polysaccharides (the more dominant functional groups) and/or proteins work as reductants, whereas fatty acids and/or polysaccharides represent stabilizing agents during the synthesis of NPs. Intriguingly, B-P@Ag-NPs were distinguished by other groups, including N−O, C−C=C, and S=O, suggesting that these functional groups may also precipitate during the synthesis of B-P@Ag-NPs. Intriguingly, the presence of sulfur was detected by EDX analysis of the B-P@Ag-NPs. The FTIR data corresponded to the GC−MS data, in which the dominant volatile compounds were fatty acids. Gallón et al. showed that the FTIR spectra of Ag-NPs synthesized by expo-polysaccharides located at 3390, 3382, 3363, and 3351 cm^{-1} related to O−H stretching of polysaccharides, 1645, 1635, 1646, and 1648 cm^{-1} representing C=O stretching and the band at 1400 cm^{-1} approved the presence of a carboxylic group, while bands at 2960−2850 cm^{-1} referring to C−H stretching of the methyl and methylene which usually exist in glucose or galactose suggest that polysaccharides were responsible for reducing and stabilizing Ag-NPs.[46]

Biological Activity of B-P@Ag-NPs and S-P@Ag-NPs. *Anticancer Activity.* B-P@Ag-NPs and S-P@Ag-NPs exhibited significant antitumor activity against colon and breast cancers with low toxicity against human fibroblast cell lines (Figure
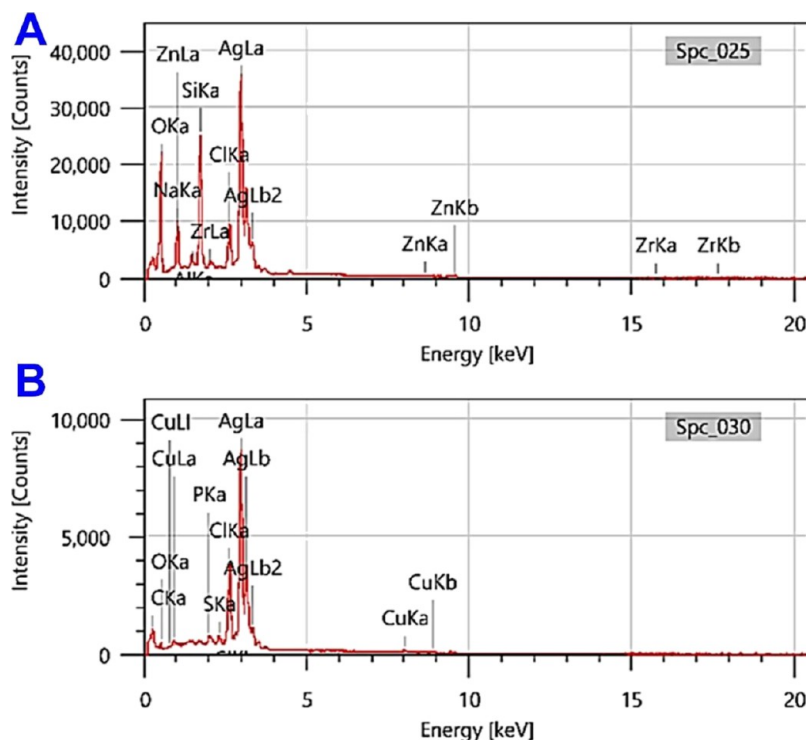

Figure 8. EDX graphs illustrating the elemental compositions of S-P@Ag-NPs (A) and B-P@Ag-NPs (B) synthesized by cell-free medium and *P. laetevirens* biomass extract.
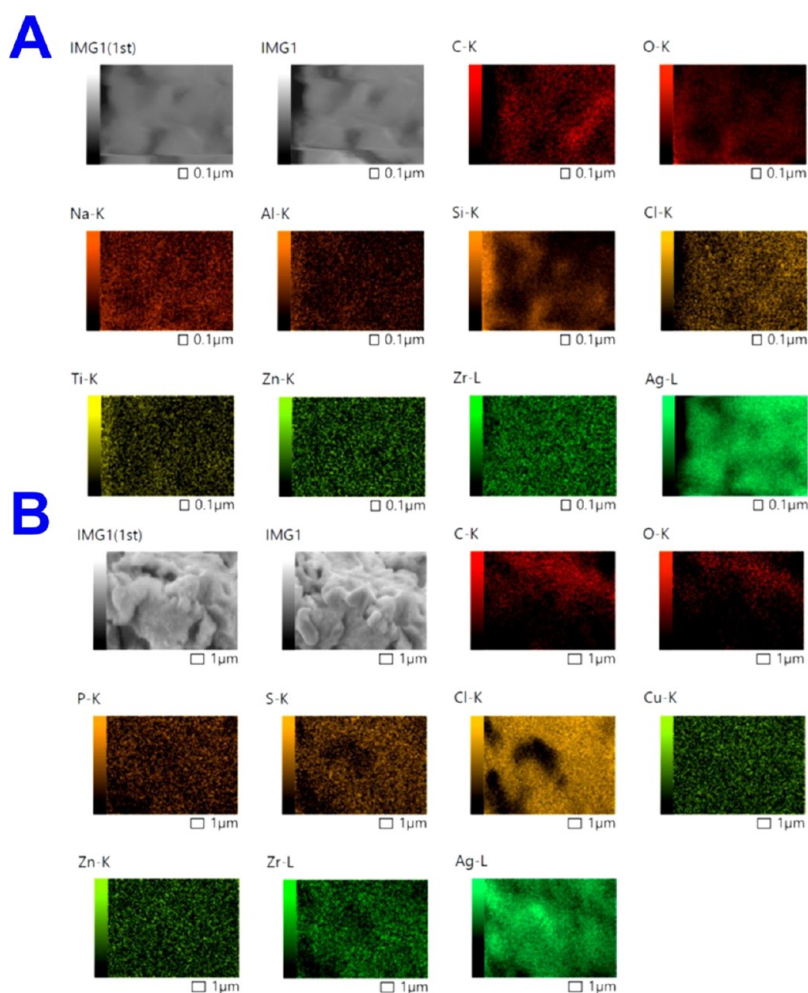
Figure 9. Mapping analyses of S-P@Ag-NPs (A) and B-P@Ag-NPs (B) synthesized by cell-free medium and *P. laetevirens* biomass extract.

Table 2. Elemental Compositions of S-P@Ag-NPs (A) and B-P@Ag-NPs (B) Synthesized by Cell-Free Medium and *P. laetevirens* Biomass Extract

element	line	mass%	atom%	element	line	mass%	atom%
O	K	23.47 ± 0.06	55.09 ± 0.14	C	K	5.40 ± 0.04	26.37 ± 0.20
Na	K	4.20 ± 0.02	6.85 ± 0.04	O	K	2.58 ± 0.06	9.47 ± 0.22
Al	K	0.84 ± 0.01	1.17 ± 0.02	P	K	0.74 ± 0.03	1.41 ± 0.05
Si	K	9.07 ± 0.03	12.12 ± 0.04	S	K	0.99 ± 0.02	1.80 ± 0.04
Cl	K	3.51 ± 0.02	3.72 ± 0.02	Cl	K	9.90 ± 0.06	16.39 ± 0.10
Zn	K	1.97 ± 0.06	1.13 ± 0.03	Cu	K	2.20 ± 0.12	2.03 ± 0.11
Zr	L	1.34 ± 0.03	0.55 ± 0.01	Ag	L	78.19 ± 0.26	42.53 ± 0.14
Ag	L	55.61 ± 0.09	19.36 ± 0.03				
total		100.00	100.00	total		100.00	100.00

12). The data showed that B-P@Ag-NPs significantly reduced the viability of Sw620, HT-29, MDA-MB231, MCF-7, and HFs by 50% at 4.1, 50.6, 26.5, 34.2, and 55.8 µg/mL, respectively. Sw620 cell line was the most permeable to B-P@Ag-NPs compared to other tested cells, while HFs showed the lowest response to B-P@Ag-NPs compared to other tested cells. Among the malignant cells, HT-29 cells were the most resistant to B-P@Ag-NPs. These results demonstrate that B-P@Ag-NPs have significant antiproliferative activity against both breast and colon cancer cells at lower concentrations and good biocompatibility against HFs cells at the same concentrations. In contrast, the antitumor activity of the B-P@Ag-NPs was dependent on the cancer cell type. For

instance, among colon cancer cells, Sw620 was the most sensitive cell line, whereas MDA-MB231 cells were the most responsive to B-P@Ag-NPs compared to MCF-7 cells. This may be related to the nature of malignant cells (metabolism, genetics, mutations, etc.) and how the cells interact with NPs, starting from the outside barrier (plasma membrane) to the mechanistic pathway of NPs inside the cells.[54] The algal corona-surrounded NPs surface controls the therapeutic activity of the NPs themselves.[55] The chemical structure of the algal corona surrounding the NPs may include proteins, fatty acids, vitamins, and secondary metabolites. One or more of these molecules may have a high affinity for Sw620 (in the case of B-P@Ag-NPs) or HT-29 (in the case of S-P@Ag-NPs)
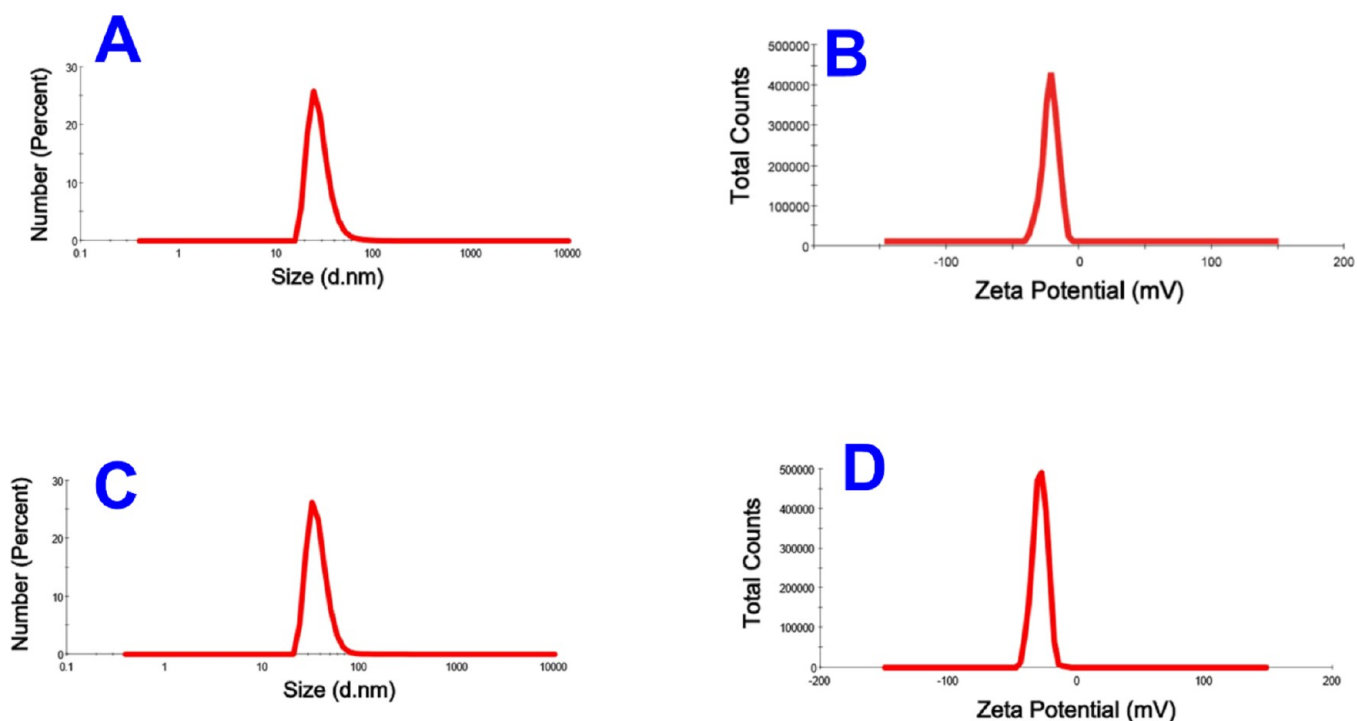
Figure 10. Hydrodynamic diameter and zeta potential of S-P@Ag-NPs (A and B) and B-P@Ag-NPs (C and D) synthesized by cell-free medium and *P. laetevirens* biomass extract, respectively.

Table 3. Hydrodynamic Diameter and Zeta Potential of B-P@Ag-NPs and S-P@Ag-NPs Synthesized by *P. laetevirens* Biomass Extract and Cell-Free Medium

NPs	Zeta (mV)	size (nm)	PDI
B-P@Ag-NPs	−28.4	37.7	0.55
S-P@Ag-NPs	−26.1	28.3	0.56

cells, enabling more NPs to enter cancer cells and cause greater damage, which may have a higher potential to induce the cell death pathway in colon cancer cells than in breast cancer cells. S-P@Ag-NPs significantly inhibited 50% of Sw620, HT-29, MDA-MB231, MCF-7, and HFs cell viability at 17.3, 8.8, 30.0, 15.3, and 13.6 μg/mL, respectively. The most vulnerable cells to S-P@Ag-NPs were HT-29 cells and HFs, while MDA-MB231 cells were the most resistant cells to S-P@Ag-NPs compared to other cell lines. Based on these data, we conclude that S-P@Ag-NPs have potent inhibitory activity against both colon and breast cancers; however, their toxicity against HFs could limit their application. Similar to the B-P@Ag-NPs, the efficacy of the S-P@Ag-NPs was cell-dependent. By examining the IC_{50} of both B-P@Ag-NPs and S-P@Ag-NPs against HFs, we concluded that B-P@Ag-NPs were more biocompatible

Table 4. Functional Groups in *P. laetevirens* Biomass Extract and Cell-Free Medium and Surrounding B-P@Ag-NPs and S-P@Ag-NPs Synthesized by *P. laetevirens*

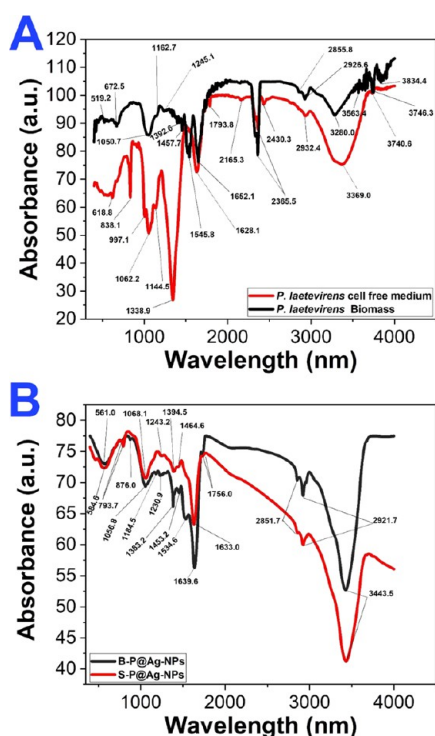| *P. laetevirens* biomass extract		B-P@Ag-NPs		Cell-free medium extract		S-P@Ag-NPs	
FTIR (cm^{-1})	functional group	FTIR (cm^{-1})	functional group	FTIR (cm^{-1})	functional group	FTIR (cm^{-1})	functional group
3834.4	O−H	3443.5	O−H	3740.6	O−H	3443.5	O−H
3746.3	O−H	2921.7	C−H	3369.0	N−H	2921.7	C−H
3563.4	O−H	2851.7	C−H	2932.4	C−H	2851.7	C−H
3280.0	O−H	1756.0	C=O	2430.3	N−H	1756.0	C=O
2926.6	C−H	1639.6	N−H	2365.6	C=C	1633.0	N−H
2855.8	C−H	1534.6	N−O	2165.3	S−C≡N	1464.6	C−H
2365.6	C=C[50]	1453.2	C=C−C	1793.8	C=O	1394.5	O−H
1793.8	C=O	1383.2	O−H	1628.1	N−H	1243.2	C−O
1652.1	N−H	1230.9	C−O	1338.9	C−N[51]	1068.1	C−O
1545.8	N−O	1184.5	S=O	1144.5	C−O	793.7	C−H
1457.7	C=C−C[52]	1056.8	C−O	1062.2	C−O	584.6	C−Br
1392.6	COO^{-}[53]	876.0	C−H	997.1	C=C		
1245.1	C−O	793.7	C−H	838.1	C=C		
1162.7	C−O	561	C−I	618.8	C−Br		
1050.7	C−O						
672.9	C=C						
519.2	C−I						

Figure 11. FTIR spectra of *P. laetevirens* biomass, cell-free medium (A), B-P@Ag-NPs and S-P@Ag-NPs (B) synthesized by *P. laetevirens* biomass extract and cell-free medium.

than S-P@Ag-NPs. This could be attributed to several hypotheses, including (i) the size of NPs (B-P@Ag-NPs have a larger size compared to S-P@Ag-NPs), as the small size of NPs easily penetrates the cell membranes and results in more toxic effects.[56] (ii) The density, chemical concentration, and nature of the algal corona layer surrounding the NPs could be significant factors in reducing toxicity by decreasing the interaction between the NPs and the protein corona, resulting in low NPs agglomeration. Veeragoni et al. reported that Ag-NPs synthesized by *Padina tetrastromatica* had a potent anticancer activity with low toxicity against the normal CHO-K1 cell line compared to chemically synthesized Ag-NPs. We attribute the high biocompatibility of the biogenic Ag-NPs to the presence of antioxidants in the *P. tetrastromatica* extract.

In addition, Ag-NPs synthesized using algal biomass may have more concentrated functional groups on their surface than Ag-NPs synthesized using a cell-free medium. These biomolecules may be antioxidants, vitamins, or fatty acids that balance the side effects of the NPs themselves. By comparing the IC_{50} of both B-P@Ag-NPs and S-P@Ag-NPs against all tested cells, it can be concluded that both NPs have selective anticancer activities that may depend on the size of the NPs, the algal corona surrounding the NPs, and the nature of the cancer cells. Additionally, both B-P@Ag-NPs and S-P@Ag-NPs exhibited greater antiproliferative activity against colon cancer cells than against breast cancer cells. These data suggest that both B-P@Ag-NPs and S-P@Ag-NPs could be used as potent anticancer agents against Sw620 and HT-29 cancer cells, with high biocompatibility against normal HFs cells. However, further studies are required to understand the molecular mechanisms of these NPs in cancer cells. 5-FU caused 50% cell growth inhibition in Sw620, HT-29, MDA-

MB231, MCF-7, and HFs cells at 1000, 1000, 442.7, 56.48, and 32.4 μg/mL, respectively, while Ch@Ag-NPs resulted in 50% cell growth inhibition at 155.0, 800.8, 256.9, 31.18, and 54.06 μg/mL (Figure 13). These data demonstrate that both B-P@Ag-NPs and S-P@Ag-NPs have greater anticancer activity against colon and breast cancers than 5-FU and the chemically synthesized Ag-NPs. Ag-NPs (nanosize of 62.7 ± 0.25 nm and a spherical shape) produced by *Gracilaria edulis* inhibited MDA-MB-231 cell growth at an IC_{50} of 344.27 ± 2.56 μg/mL,[57] while Ag-NPs synthesized by *Anabaena doliolum* inhibited 50% of Dalton's lymphoma and human colon carcinoma colo205 cell proliferation at low concentrations (20 μg/mL),[58] while Ag-NPs synthesized by Nostoc sp. strain HKAR-2 suppressed the proliferation activity of MCF-7 cells at IC_{50} of 27.5 μg/mL.[59]

Antibacterial Activity. B-P@Ag-NPs and S-P@Ag-NPs inhibited the growth of *B. cereus*, *B. subtilis*, and *E. coli* at lower MIC and MBC, as shown in Table 5. Except for ciprofloxacin, the data from the inhibition zone (IZ, Table) demonstrated that B-P@Ag-NPs had stronger inhibitory activity against the tested strains than S-P@Ag-NPs, AgNO₃, and Ch@Ag-NPs (Figure 14). Although B-P@Ag-NPs were larger than S-P@Ag-NPs, their biocidal influence was greater. These data could be attributed to the following: (i) The density and concentration of functional groups derived from microalgae that surround the NPs enhanced their biocidal potential by facilitating the entry of NPs into cells through interactions with bacterial membranes.[55] (ii) The algal biomolecule-coated NPs exhibited antibacterial activity at higher concentrations.[55] (iii) The larger size of the B-P@Ag-NPs may increase their toxicity against bacterial isolates by interfering with the bacterial efflux process. Although both B-P@Ag-NPs and S-P@Ag-NPs have a negative charge on their surfaces, they demonstrated superior activity against Gram-negative bacteria compared to Gram-positive bacteria. Herein, we concluded that the potential charge may not influence the biocidal activity of either NPs. It could be that there are factors other than potential charge controlling the biocidal effects of biogenic NPs, including nanosize, biogenic materials surrounding NPs, and bacterial structure and response mechanism; however, this does not cancel the role of the NPs charge in increasing the chance of NPs negatively impacting bacterial growth through an attractive electric force between NPs and the bacterial surfaces. Researchers have explained this phenomenon based on the fact that Gram-positive bacteria have a thicker wall composed of thick peptidoglycan (~30 nm) compared with the thin wall layer of Gram-negative bacteria (~3 nm). This thickness can facilitate the cellular internalization of the NPs. Another hypothesis is that the strong negative charge of teichoic and lipoteichoic acids, which are also components of the cell wall of Gram-positive bacteria, may bind to and sequester free silver ions.[60] On the other hand, a comparison of the IZ values of bacteria treated with Ch@Ag-NPs, B-P@Ag-NPs, and S-P@Ag-NPs showed that the algal functional groups surrounding B-P@Ag-NPs and S-P@Ag-NPs played a major role in making them more biocidal than Ch@Ag-NPs. B-P@Ag-NPs exhibited greater antibacterial activity against *B. cereus*, *B. subtilis*, and *E. coli* compared to AgNO₃. The S-P@Ag-NPs also showed a greater inhibitory effect against *B. cereus* and *E. coli* bacteria compared to AgNO₃ while causing an approximately similar response to AgNO₃ against *B. subtilis*. These data could be attributed to the smaller size of B-P@Ag-NPs and S-P@Ag-NPs, which enhanced their ther-
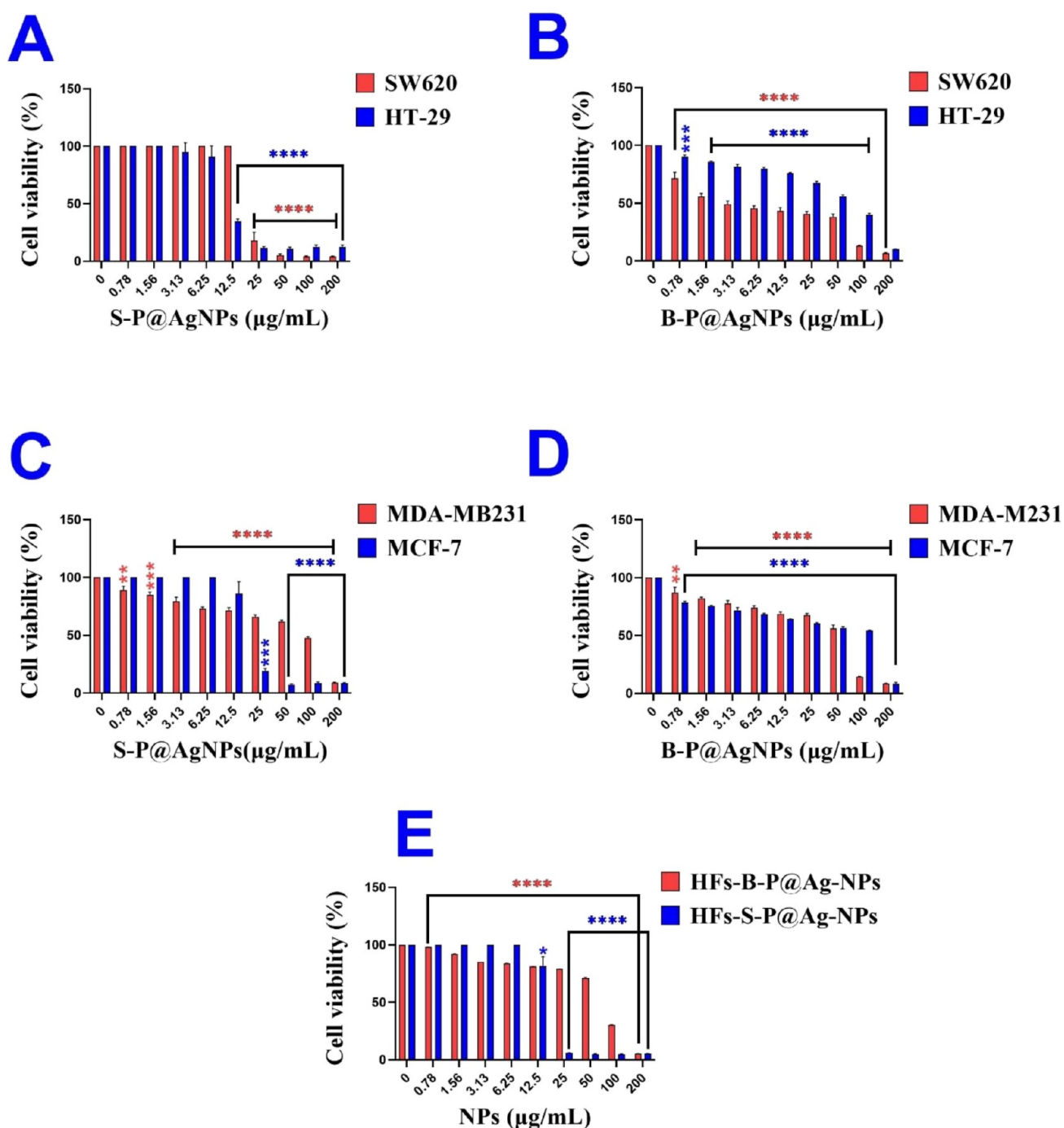
Figure 12. Cell viability of Sw620, HT-29 (A and B), MDA-MB-231, MCF-7 (C and D), and HFs (E) before and after being treated with S-P@Ag-NPs and B-P@Ag-NPs synthesized by cell-free medium and *P. laetevirens* biomass extract.

apeutic activity, and/or the new nanoformulation of Ag-NPs and algal corona, which increased the biocidal activity, with which NPs worked as drug vehicles for algal biomolecules. Gallón et al. synthesized Ag-NPs using exopolysaccharides of *Botryococcus braunii* and *Chlorella pyrenoidosa* with a nanosize between 5 and 15 nm and a negative charge on their surfaces. The Ag-NPs showed potent antibacterial activity against *E. coli*, *Staphylococcus aureus*, and methicillin-resistant *Staphylococcus aureus* (MRSA). Regardless of the size of the tested Ag-NPs, the most significant antibacterial effect was detected against Gram-negative bacteria.[46] Khan et al. synthesized silver-capped magnesium oxide nanocomposite using Olea cuspidata leaf

extract which killed 99% of *E. coli* and *S. aureus* bacterial cells at 15 and 20 μg/mL, respectively.[61] Bishoyi et al. synthesized AgNPs using *Oscillatoria princeps* and assessed its antibacterial activity against *MRSA*, *S. pyogenes* and *E. coli*.[62] The authors reported that MIC values of AgNPs against *MRSA*, *S. pyogenes*, and *E. coli* were 100, 80, and 60 μg/mL, respectively. Additionally, the MIC values of AgNPs synthesized by *Leptolyngbya* sp. WUC 59 against *B. subtilis* and *E. coli* were 8 mg/mL, suggesting their potential as a bactericidal agent.[63] By comparing these data with the existing MIC data for S-P@Ag-NPs and B-P@Ag-NPs (Table 5). We concluded that S-P@Ag-NPs and B-P@Ag-NPs synthesized by novel *P. laetevirens*
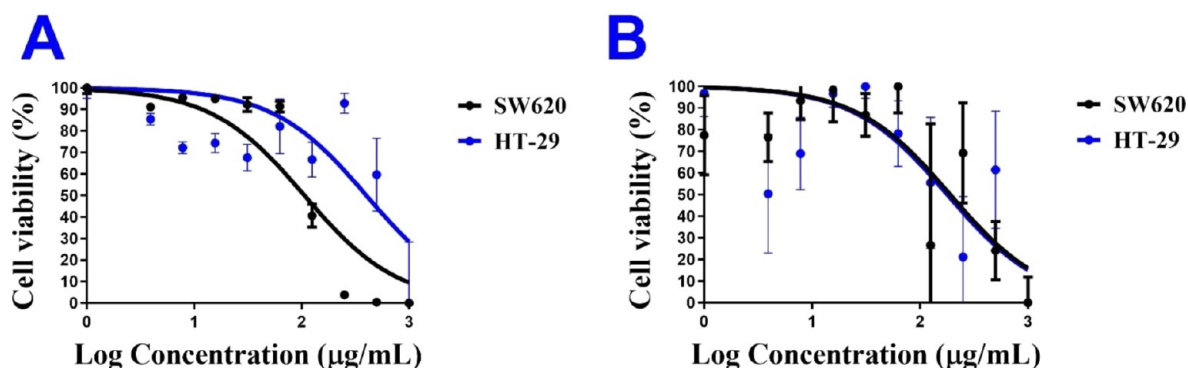
Figure 13. Antiproliferative activity of 1000 μg/mL of Ch@Ag-NPs (A) and 5-FU (B) against Sw620 and HT-29 cells.

Table 5. Minimum Inhibition and Maximum Biocidal Concentrations (μg/mL) of B-P@Ag-NPs and S-P@Ag-NPs and Inhibition Zone (mm) of Ciprofloxacin, B-P@Ag-NPs, S-P@Ag-NPs, AgNO₃, and Ch@Ag-NPs against *B. cereus*, *B. subtilis*, and *E. coli*

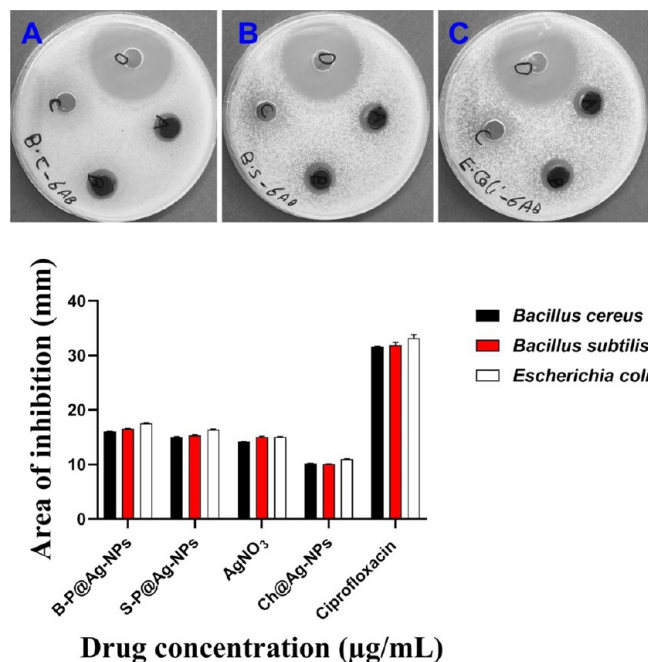| drugs	*Bacillus cereus*		*Bacillus subtilis*		*Escherichia coli*	
	MIC	MBC	MIC	MBC	MIC	MBC
B-P@Ag-NPs	31.3	62.5	31.3	62.5	31.3	62.5
S-P@Ag-NPs	7.81	15.62	7.81	15.62	1.95	3.90
	inhibition zone (mm)					
B-P@Ag-NPs	16.0 ± 0.05		16.5 ± 0.1		17.5 ± 0.1	
S-P@Ag-NPs	15.0 ± 0.1		15.3 ± 0.1		16.4 ± 0.1	
AgNO₃	14.2 ± 0.03		15.0 ± 0.19		15.0 ± 0.13	
Ch@Ag-NPs	10.2 ± 0.03		10.1 ± 0.03		11.0 ± 0.05	
ciprofloxacin	31.6 ± 0.1		31.9 ± 0.5		33.2 ± 0.6	

Figure 14. Biocidal activity of ciprofloxacin (5 μg/mL), B-P@Ag-NPs, S-P@Ag-NPs, and Ch@Ag-NPs (1000 μg/mL) against *B. cereus*, *B. subtilis*, and *E. coli*.

have more efficacy and higher bactericidal activity at lower concentrations.

CONCLUSIONS

The current findings are the first to demonstrate the potential of *P. laetevirens* to reduce and stabilize Ag-NPs and to report the main phytochemicals of *P. laetevirens* precipitated during the biofabrication of NPs. Two extracellular synthesis methods for Ag-NPs using *P. laetevirens* biomass extract and cell-free medium were developed by controlling abiotic parameters, including precursor concentrations and ratios, temperature, time of exposure to temperature, pH, illumination, and incubation time, to produce stable, small, and uniform Ag-NPs. The data revealed that both *P. laetevirens* biomass extract and cell-free medium had the potential to synthesize Ag-NPs with a small nanosize, a negative charge on their surface, and good stability. Physical and chemical parameters such as temperature, light energy, AgNO₃ concentration, and pH significantly influenced the size and stability of the NPs. This implies that, when biologically synthesizing NPs using microalgae, it is preferable to optimize the reaction to control their physicochemical properties. The main functional groups in both *P. laetevirens* biomass extract and cell-free medium were O−H, C−H, N−H, and C−O groups, suggesting that polysaccharides and proteins act as reductants, while polysaccharides/fatty acids represent stabilizing agents during the synthesis of NPs. GC−MS analysis showed that *P. laetevirens* contained a wide range of fatty acids and esters, which could be the main chemicals for stabilizing NPs. B-P@Ag-NPs and S-P@Ag-NPs showed significant anticancer activity against colon and breast cancers; however, the biocompatibility of B-P@Ag-NPs was higher than that of S-P@Ag-NPs against HFs. B-P@Ag-NPs and S-P@Ag-NPs showed greater antiproliferative activity against colon cancer cells than against breast cancer cells. B-P@Ag-NPs and S-P@Ag-NPs exhibited greater biocidal activity against Gram-negative bacteria than against Gram-positive bacteria. These findings suggest that *P. laetevirens* is a sustainable source of Ag-NPs that can be used as a potent therapeutic agent against cancer and infectious diseases.

AUTHOR INFORMATION

Corresponding Author

Alya Redhwan − *Department of Heath, College of Health, and Rehabilitation Sciences, Princess Nourah bint Abdulrahman University, Riyadh 11671, Saudi Arabia*; Phone: +966-0118240627; Email: AMRedhwan@pnu.edu.sa

Authors

Reham Samir Hamida − *Institute for Protein Research, Osaka University, Osaka 565-0871, Japan;* ● orcid.org/0000-0003-2441-6599

Mohamed Abdelaal Ali − *Plant Production Department, Arid Lands Cultivation Research Institute, City of Scientific Research and Technological Applications (SRTA-CITY) New Borg El-Arab, Alexandria 21934, Egypt*

Njoud Mugren − *Graduated Student, Department of Chemistry, College of Science, Princess Nourah bint Abdulrahman University, Riyadh 11671, Saudi Arabia*

Mayasar Ibrahim Al-Zaban − *Department of Biology, College of Science, Princess Nourah bint Abdulrahman University, Riyadh 11671, Saudi Arabia*

Mashael Mohammed Bin-Meferij − *Department of Biology, College of Science, Princess Nourah bint Abdulrahman University, Riyadh 11671, Saudi Arabia*

Complete contact information is available at:
https://pubs.acs.org/10.1021/acsomega.3c02368

■ REFERENCES

(1) (a) Alexander, J. W. History of the medical use of silver. *Surg. Infect.* **2009**, *10*, 289−292. (b) Barillo, D. J.; Marx, D. E. Silver in medicine: A brief history BC 335 to present. *Burns* **2014**, *40*, S3−S8. (c) Sabarees, G.; Velmurugan, V.; Tamilarasi, G. P.; Alagarsamy, V.; Raja Solomon, V. Recent Advances in Silver Nanoparticles Containing Nanofibers for Chronic Wound Management. *Polymer* **2022**, *14*, 3994.

(2) Xu, L.; Yi-Yi, W.; Huang, J.; Chun-Yuan, C.; Zhen-Xing, W.; Xie, H. Silver nanoparticles: Synthesis, medical applications and biosafety. *Theranostics* **2020**, *10*, 8996.

(3) Ahmad, S. A.; Das, S. S.; Khatoon, A.; Ansari, M. T.; Afzal, M.; Hasnain, M. S.; Nayak, A. K. Bactericidal activity of silver nanoparticles: A mechanistic review. *Mater. Sci. Energy Technol.* **2020**, *3*, 756−769.

(4) Jian, Y.; Chen, X.; Ahmed, T.; Shang, Q.; Zhang, S.; Ma, Z.; Yin, Y. Toxicity and action mechanisms of silver nanoparticles against the mycotoxin-producing fungus Fusarium graminearum. *J. Adv. Res.* **2022**, *38*, 1−12.

(5) Pan, X.; Zhang, Y.; Zhao, Y.; Yao, S.; Guan, C.; Wang, L.; Chen, L. Inhibitory activity and mechanism of silver nanoparticles against herpes simplex virus type 1. *Arch. Virol.* **2022**, *167*, 1619−1636.

(6) Miranda, R. R.; Sampaio, I.; Zucolotto, V. Exploring silver nanoparticles for cancer therapy and diagnosis. *Colloids Surf., B* **2022**, *210*, No. 112254.

(7) Shanmuganathan, R.; Karuppusamy, I.; Saravanan, M.; Muthukumar, H.; Ponnuchamy, K.; Ramkumar, V. S.; Pugazhendhi, A. Synthesis of silver nanoparticles and their biomedical applications-a comprehensive review. *Curr. Pharm. Des.* **2019**, *25*, 2650−2660.

(8) (a) Arjun, P. N. J.; Sankar, B.; Shankar, K. V.; Kulkarni, N. V.; Sivasankaran, S.; Shankar, B. Silver and Silver Nanoparticles for the Potential Treatment of COVID-19: A Review. *Coatings* **2022**, *12*, 1679. (b) Miu, B. A.; Dinischiotu, A. New Green Approaches in Nanoparticles Synthesis: An Overview. *Molecules* **2022**, *27*, 6472.

(9) Hamida, R. S.; Ali, M. A.; Redhwan, A.; Bin-Meferij, M. M. Cyanobacteria−a promising platform in green nanotechnology: a review on nanoparticles fabrication and their prospective applications. *Int. J. Nanomed.* **2020**, 6033−6066.

(10) Dağlıoğlu, Y.; Yılmaz Öztürk, B. A novel intracellular synthesis of silver nanoparticles using Desmodesmus sp.(Scenedesmaceae): different methods of pigment change. *Rend. Fis. Acc. Lincei* **2019**, *30*, 611−621.

(11) Khan, A. U.; Khan, A. U.; Li, B.; Mahnashi, M. H.; Alyami, B. A.; Alqahtani, Y. S.; Tahir, K.; Khan, S.; Nazir, S. A facile fabrication of silver/copper oxide nanocomposite: An innovative entry in photocatalytic and biomedical materials. *Photodiagn. Photodyn. Ther.* **2020**, *31*, No. 101814.

(12) Hayat, P.; Khan, I.; Rehman, A.; Jamil, T.; Hayat, A.; Rehman, M. U.; Ullah, N.; Sarwar, A.; Alharbi, A. A.; Dablool, A. S.; Daudzai, Z.; Alamri, A. S.; Alhomrani, M.; Aziz, T. Myogenesis and Analysis of Antimicrobial Potential of Silver Nanoparticles (AgNPs) against Pathogenic Bacteria. *Molecules* **2023**, *28*, 637.

(13) Zdenka, B.; Matej, B.; Aneta, S.; Michal, G. Synthesis of metal nanoparticles using lichens and their biological applications. In *Fungal Cell Factories for Sustainable Nanomaterials Productions and Agricultural Applications*; Elsevier, 2023; pp 163−203.

(14) Ahmad, W.; Khan, A. U.; Shams, S.; Qin, L.; Yuan, Q.; Ahmad, A.; Wei, Y.; Khan, Z. U. H.; Ullah, S.; Rahman, A. U. Eco-benign approach to synthesize spherical iron oxide nanoparticles: A new insight in photocatalytic and biomedical applications. *J. Photochem. Photobiol., B* **2020**, *205*, No. 111821.

(15) (a) Princy, K.; Gopinath, A. Optimization of physicochemical parameters in the biofabrication of gold nanoparticles using marine macroalgae Padina tetrastromatica and its catalytic efficacy in the degradation of organic dyes. *J. Nanostructure Chem.* **2018**, *8*, 333−342. (b) Thamilselvi, V.; Radha, K. Synthesis of silver nanoparticles from Pseudomonas putida NCIM 2650 in silver nitrate supplemented growth medium and optimization using response surface methodology. *Dig. J. Nanomater. Biostructures* **2013**, *8*, 1101−1111.

(16) Hamida, R. S.; Ali, M. A.; Alkhateeb, M. A.; Alfassam, H. E.; Momenah, M. A.; Bin-Meferij, M. M. Algal-Derived Synthesis of Silver Nanoparticles Using the Unicellular ulvophyte sp. MBIC10591: Optimisation, Characterisation, and Biological Activities. *Molecules* **2023**, *28*, 279.

(17) Sharma, D.; Kanchi, S.; Bisetty, K. Biogenic synthesis of nanoparticles: a review. *Arab. J. Chem.* **2019**, *12*, 3576−3600.

(18) Khan, F.; Shahid, A.; Zhu, H.; Wang, N.; Javed, M. R.; Ahmad, N.; Xu, J.; Alam, M. A.; Mehmood, M. A. Prospects of algae-based green synthesis of nanoparticles for environmental applications. *Chemosphere* **2022**, *293*, No. 133571.

(19) Zayadi, R. A.; Bakar, F. A. Comparative study on stability, antioxidant and catalytic activities of bio-stabilized colloidal gold nanoparticles using microalgae and cyanobacteria. *J. Environ. Chem. Eng.* **2020**, *8*, No. 103843.

(20) Araya-Castro, K.; Chao, T.-C.; Durán-Vinet, B.; Cisternas, C.; Ciudad, G.; Rubilar, O. Green synthesis of copper oxide nanoparticles using protein fractions from an aqueous extract of Brown Algae Macrocystis pyrifera. *Processes* **2021**, *9*, 78.

(21) Caliskan, G.; Mutaf, T.; Agba, H. C.; Elibol, M. Green Synthesis and Characterization of Titanium Nanoparticles Using

Microalga, Phaeodactylum tricornutum. *Geomicrobiol. J.* **2022**, *39*, 83−96.

(22) Bulgariu, L.; Bulgariu, D. Bioremediation of toxic heavy metals using marine algae biomass. *Green Mater. Wastewater Treat.* **2020**, 69−98.

(23) Mmola, M.; Roes-Hill, M. L.; Durrell, K.; Bolton, J. J.; Sibuyi, N.; Meyer, M. E.; Beukes, D. R.; Antunes, E. Enhanced antimicrobial and anticancer activity of silver and gold nanoparticles synthesised using Sargassum incisifolium aqueous extracts. *Molecules* **2016**, *21*, 1633.

(24) Chokshi, K.; Pancha, I.; Ghosh, T.; Paliwal, C.; Maurya, R.; Ghosh, A.; Mishra, S. Green synthesis, characterization and antioxidant potential of silver nanoparticles biosynthesized from de-oiled biomass of thermotolerant oleaginous microalgae Acutodesmus dimorphus. *RSC Adv.* **2016**, *6*, 72269−72274.

(25) Younis, N. S.; Mohamed, M. E.; El Semary, N. A. Green synthesis of silver nanoparticles by the Cyanobacteria synechocystis sp.: Characterization, antimicrobial and diabetic wound-healing actions. *Mar. Drugs* **2022**, *20*, 56.

(26) Hamida, R. S.; Ali, M. A.; Almohawes, Z. N.; Alahdal, H.; Momenah, M. A.; Bin-Meferij, M. M. Green Synthesis of Hexagonal Silver Nanoparticles Using a Novel Microalgae Coelastrella aeroterrestrica Strain BA_Chlo4 and Resulting Anticancer, Antibacterial, and Antioxidant Activities. *Pharmaceutics* **2022**, *14*, 2002.

(27) Morowvat, M. H.; Kazemi, K.; Jaberi, M. A.; Amini, A.; Gholami, A. Biosynthesis and Antimicrobial Evaluation of Zinc Oxide Nanoparticles Using Chlorella vulgaris Biomass against Multidrug-Resistant Pathogens. *Materials* **2023**, *16*, 842.

(28) Bolch, C. J.; Orr, P. T.; Jones, G. J.; Blackburn, S. I. Genetic, morphological, and toxicological variation among globally distributed strains of Nodularia (Cyanobacteria). *J. Phycol.* **1999**, *35*, 339−355.

(29) Tschaikner, A. G.; Kofler, W. Coelastrella aeroterrestrica sp. nov.(Chlorophyta, Scenedesmoideae) a new, obviously often over-looked aeroterrestrial species. *Algol. Stud.* **2008**, 11−20.

(30) Khaw, Y. S.; Khong, N. M. H.; Shaharuddin, N. A.; Yusoff, F. M. A simple 18S rDNA approach for the identification of cultured eukaryotic microalgae with an emphasis on primers. *J. Microbiol. Methods* **2020**, *172*, No. 105890.

(31) Abd El-Kareem, M. S.; Rabbih, M. A. E. F.; Selim, E. T. M.; Elsherbiny, E. A. E.-M.; El-Khateeb, A. Y. Application of GC/EIMS in combination with semi-empirical calculations for identification and investigation of some volatile components in basil essential oil. *Int. J. Anal. Mass Spectrom. Chromatogr.* **2016**, *04*, 14−25.

(32) Mosmann, T. Rapid colorimetric assay for cellular growth and survival: application to proliferation and cytotoxicity assays. *J. Immunol. Methods* **1983**, *65*, 55−63.

(33) Hamida, R. S.; Ali, M. A.; Goda, D. A.; Khalil, M. I.; Al-Zaban, M. I. Novel biogenic silver nanoparticle-induced reactive oxygen species inhibit the biofilm formation and virulence activities of methicillin-resistant Staphylococcus aureus (MRSA) strain. *Front. Bioeng. Biotechnol.* **2020**, *8*, 433.

(34) Elshikh, M.; Ahmed, S.; Funston, S.; Dunlop, P.; McGaw, M.; Marchant, R.; Banat, I. M. Resazurin-based 96-well plate micro-dilution method for the determination of minimum inhibitory concentration of biosurfactants. *Biotechnol. Lett.* **2016**, *38*, 1015−1019.

(35) (a) Škaloud, P.; Rindi, F.; Boedeker, C.; Leliaert, F. *Freshwater Flora of Central Europe, Vol 13: Chlorophyta: Ulvophyceae (Süßwasserflora von Mitteleuropa, Bd. 13: Chlorophyta: Ulvophyceae)*; Springer-Verlag, 2018. (b) Gerneck, R. Zur Kenntnis der niederen Chlorophyceen. *Beih. Bot. Centralbl.* **1907**, *21*, 221−290.

(36) (a) Senyilmaz-Tiebe, D.; Pfaff, D. H.; Virtue, S.; Schwarz, K. V.; Fleming, T.; Altamura, S.; Muckenthaler, M. U.; Okun, J. G.; Vidal-Puig, A.; Nawroth, P.; Teleman, A. A. Dietary stearic acid regulates mitochondria in vivo in humans. *Nat. Commun.* **2018**, *9*, 3129. (b) Chan, Y.; Singh, S. K.; Gulati, M.; Wadhwa, S.; Prasher, P.; Kumar, D.; Kumar, A. P.; Gupta, G.; Kuppusamy, G.; Haghi, M.; George Oliver, B. G.; Adams, J.; Chellappan, D. K.; Dua, K. Advances

and applications of monoolein as a novel nanomaterial in mitigating chronic lung diseases. *J. Drug Deliv. Sci. Technol.* **2022**, *74*, 103541.

(37) Kovalenko, M. V.; Bodnarchuk, M. I.; Lechner, R. T.; Hesser, G.; Schäffler, F.; Heiss, W. Fatty acid salts as stabilizers in size-and shape-controlled nanocrystal synthesis: the case of inverse spinel iron oxide. *J. Am. Chem. Soc.* **2007**, *129*, 6352−6353.

(38) Sobczak-Kupiec, A.; Malina, D.; Wzorek, Z.; Zimowska, M. Influence of silver nitrate concentration on the properties of silver nanoparticles. *Micro Nano Lett.* **2011**, *6*, 656−660.

(39) Kim, C. W.; Jeong, H.; Noh, Y.; Lee, D.; Lee, C.; Jin, C. Influence of the Chemical Molar Ratio on the Copper Nanoparticles: Controlled-Surfactants,-Reducing Agents, and-Precursors. *Bull. Korean Chem. Soc.* **2016**, *37*, 700−704.

(40) Liu, H.; Zhang, H.; Wang, J.; Wei, J. Effect of temperature on the size of biosynthesized silver nanoparticle: deep insight into microscopic kinetics analysis. *Arab. J. Chem.* **2020**, *13*, 1011−1019.

(41) Dong, C.; Zhang, X.; Cai, H.; Cao, C. Facile and one-step synthesis of monodisperse silver nanoparticles using gum acacia in aqueous solution. *J. Mol. Liq.* **2014**, *196*, 135−141.

(42) (a) Hamal, D. B.; Klabunde, K. J. Synthesis, characterization, and visible light activity of new nanoparticle photocatalysts based on silver, carbon, and sulfur-doped TiO2. *J. Colloid Interface Sci.* **2007**, *311*, 514−522. (b) Ball, R.; Weitz, D.; Witten, T.; Leyvraz, F. Universal kinetics in reaction-limited aggregation. *Phys. Rev. Lett.* **1987**, *58*, 274.

(43) Rycenga, M.; Cobley, C. M.; Zeng, J.; Li, W.; Moran, C. H.; Zhang, Q.; Qin, D.; Xia, Y. Controlling the synthesis and assembly of silver nanostructures for plasmonic applications. *Chem. Rev.* **2011**, *111*, 3669−3712.

(44) Gontijo, L. A. P.; Raphael, E.; Ferrari, D. P. S.; Ferrari, J. L.; Lyon, J. P.; Schiavon, M. A. pH effect on the synthesis of different size silver nanoparticles evaluated by DLS and their size-dependent antimicrobial activity. *Matéria (Rio de Janeiro)* **2020**, *25*, No. e12845.

(45) Zhao, X.; Xia, Y.; Li, Q.; Ma, X.; Quan, F.; Geng, C.; Han, Z. Microwave-assisted synthesis of silver nanoparticles using sodium alginate and their antibacterial activity. *Colloids Surf., A* **2014**, *444*, 180−188.

(46) Gallón, S. M. N.; Alpaslan, E.; Wang, M.; Larese-Casanova, P.; Londoño, M. E.; Atehortúa, L.; Pavón, J. J.; Webster, T. J. Characterization and study of the antibacterial mechanisms of silver nanoparticles prepared with microalgal exopolysaccharides. *Mater. Sci. Eng., C* **2019**, *99*, 685−695.

(47) Kusumaningrum, H. P.; Zainuri, M.; Marhaendrajaya, I.; Subagio, A. Nanosilver microalgae biosynthesis: Cell appearance based on SEM and EDX methods. *J. Phys.: Conf. Ser.* **2018**, *1025*, No. 012084.

(48) Miškovská, A.; Rabochová, M.; Michailidu, J.; Masák, J.; Čejková, A.; Lorinčík, J.; Maťátková, O. Antibiofilm activity of silver nanoparticles biosynthesized using viticultural waste. *PLoS One* **2022**, *17*, No. e0272844.

(49) Roychoudhury, P.; Gopal, P. K.; Paul, S.; Pal, R. Cyanobacteria assisted biosynthesis of silver nanoparticles—a potential antileukemic agent. *J. Appl. Phycol.* **2016**, *28*, 3387−3394.

(50) Pandian, S.; Kunjiappan, S.; Ravishankar, V.; Sundarapandian, V. Synthesis of quercetin-functionalized silver nanoparticles by rapid one-pot approach. *BioTechnologia* **2021**, *102*, 75−84.

(51) Tufail, M. S.; Liaqat, I.; Andleeb, S.; Naseem, S.; Zafar, U.; Sadiqa, A.; Liaqat, I.; Ali, N. M.; Bibi, A.; Arshad, N.; Saleem, G. Biogenic synthesis, characterization and antibacterial properties of silver nanoparticles against human pathogens. *J. Oleo Sci.* **2022**, *71*, 257−265.

(52) Paralikar, P. Fabrication of ketoconazole nanoparticles and their activity against Malassezia furfur. *Nusantara Biosci.* **2016**, *7*, 43−47.

(53) Xu, L.; Fang, Y. Temperature-induced effect on surface-enhanced Raman scattering of p, m-hydroxybenzoic acid on silver nanoparticles. *Spectroscopy* **2003**, *18*, 26−31.

(54) (a) Levatić, J.; Salvadores, M.; Fuster-Tormo, F.; Supek, F. Mutational signatures are markers of drug sensitivity of cancer cells. *Nat. Commun.* **2022**, *13*, 2926. (b) Zaal, E. A.; Berkers, C. R. The

influence of metabolism on drug response in cancer. *Front. Oncol.* **2018**, *8*, 500.

(55) Roy, A.; Bulut, O.; Some, S.; Mandal, A. K.; Yilmaz, M. D. Green synthesis of silver nanoparticles: biomolecule-nanoparticle organizations targeting antimicrobial activity. *RSC Adv.* **2019**, *9*, 2673−2702.

(56) Jahan, I.; Erci, F.; Isildak, I. Facile microwave-mediated green synthesis of non-toxic copper nanoparticles using Citrus sinensis aqueous fruit extract and their antibacterial potentials. *J. Drug Deliv. Sci. Technol.* **2021**, *61*, No. 102172.

(57) Mohanta, Y. K.; Mishra, A. K.; Nayak, D.; Patra, B.; Bratovcic, A.; Avula, S. K.; Mohanta, T. K.; Murugan, K.; Saravanan, M. Exploring Dose-Dependent Cytotoxicity Profile of Gracilaria edulis-Mediated Green Synthesized Silver Nanoparticles against MDA-MB-231 Breast Carcinoma. *Oxid. Med. Cell. Longevity* **2022**, *2022*, No. 3863138.

(58) Singh, G.; Babele, P. K.; Shahi, S. K.; Sinha, R. P.; Tyagi, M. B.; Kumar, A. Green synthesis of silver nanoparticles using cell extracts of Anabaena doliolum and screening of its antibacterial and antitumor activity. *J. Microbiol. Biotechnol.* **2014**, *24*, 1354−1367.

(59) Sonker, A. S.; Pathak, J.; Kannaujiya, V. K.; Sinha, R. P. Characterization and in vitro antitumor, antibacterial and antifungal activities of green synthesized silver nanoparticles using cell extract of Nostoc sp. strain HKAR-2. *Can. J. Biotechnol.* **2017**, *1*, 26.

(60) Cavassin, E. D.; de Figueiredo, L. F. P.; Otoch, J. P.; Seckler, M. M.; de Oliveira, R. A.; Franco, F. F.; Marangoni, V. S.; Zucolotto, V.; Levin, A. S. S.; Costa, S. F. Comparison of methods to detect the in vitro activity of silver nanoparticles (AgNP) against multidrug resistant bacteria. *J. Nanobiotechnology* **2015**, *13*, 1−16.

(61) Khan, A. U.; Khan, A. U.; Li, B.; Mahnashi, M. H.; Alyami, B. A.; Alqahtani, Y. S.; Alqarni, A. O.; Khan, Z. U. H.; Ullah, S.; Wasim, M.; Khan, Q. U.; Ahmad, W. Biosynthesis of silver capped magnesium oxide nanocomposite using Olea cuspidata leaf extract and their photocatalytic, antioxidant and antibacterial activity. *Photodiagn. Photodyn. Ther.* **2021**, *33*, No. 102153.

(62) Bishoyi, A. K.; Sahoo, C. R.; Sahoo, A. P.; Padhy, R. N. Bio-synthesis of silver nanoparticles with the brackish water blue-green alga Oscillatoria princeps and antibacterial assessment. *Appl. Nanosci.* **2021**, *11*, 389−398.

(63) Singh, Y.; Kaushal, S.; Sodhi, R. S. Biogenic synthesis of silver nanoparticles using cyanobacterium Leptolyngbya sp. WUC 59 cell-free extract and their effects on bacterial growth and seed germination. *Nanoscale Adv.* **2020**, *2*, 3972−3982.